Investigation of Unusual Oxidation State and Spin State Transition in Rare Earth Transition Metal oxides

A thesis submitted in partial fulfillment
for the degree of

Master of Science

as a part of the
Integrated Ph. D. programme
(Materials Science)

by

Abhijit Sen

Chemistry and Physics of Materials Unit
Jawaharlal Nehru Centre for Advanced
Scientific Research
(A Deemed University)
Bangalore, India.

March 2014

Dedicated to my Family

DECLARATION

I hereby declare that the matter embodied in this M.S. thesis entitled **"Investigation of Unusual Oxidation State and Spin State Transition in Rare Earth Transition Metal oxides"** is the outcome of investigations carried out by me under the supervision of Prof. A. Sundaresan at the Chemistry and Physics of Materials Unit, Jawaharlal Nehru Centre for Advanced Scientific Research, Bangalore, India and this work is unique being submitted nowhere else for the award of any degree or diploma.

Thus going with the pre-existing practice of reporting scientific observations, due acknowledgement has been made whenever a work represented mentioned is based on the findings of other investigators.

31/03/2014

Abhijit Sen

Abhijit Sen

CERTIFICATE

I hereby certify that the matter embodied in this M.S. thesis entitled **"Investigation of Unusual Oxidation State and Spin State Transition in Rare Earth Transition Metal oxides"** has been carried out by Mr. Abhijit Sen at the Chemistry and Physics of Materials Unit, Jawaharlal Nehru Centre for Advanced Scientific Research, Bangalore, India under my supervision and it has not been submitted elsewhere for the award of any degree or diploma.

31/03/2014

Prof. A. Sundaresan

(Research Supervisor)

Acknowledgements

I am highly grateful to my supervisor *Prof. A. Sundaresan* for being helpful to me all the time with generous guidance and constant encouragement. So I take this opportunity to express my immense gratitude to him. I sincerely thank him for providing interesting research problems and freedom to perform all my experiments. It has been a great pleasure for me to work under his guidance. I thank him for treating me as a family member and supporting me during my thesis work.

Prof. C. N. R. Rao, FRS has been a great source of inspiration during my MS work. I would like to sincerely thank him for providing us all the experimental facilities.

I convey my sincere thanks to past and present CPMU chairmen, *Prof. G. U. Kulkarani* and *Prof. Balasubramanian* for providing all the experimental facilities.

I thank the past and present Int. Ph. D. conveners, *Prof. S. Balasubramanian* and *Dr. T. K. Maji*.

My heartfelt thanks to all my lab mates, Dr. Rambabu, Mr. Nitesh, Mr. Rana, Mr. Somnath, Mr. Chandan for giving me a friendly atmosphere in lab, guiding me for my research problem, helping me through the whole period to learn various measurement techniques and their constant support for my work.

I would like to express my sincere gratitude to all the faculty members of the Chemistry and Physics of Materials Unit and *Prof. T.N. Guru Row* of Solid State and Structural Chemistry Unit, IISC for offering their valuable courses.

I would like to thank technical staff *Mrs. Selvi, Mr.Anil, Mr. Ala Sreenibas, Mr. Sunil, Usha madam* for their help in various techniques and difficulties.

I would like to thank my batch mates *Uttam Gupta, Rajib Sahu, Raaghesh A.V., Suchtra Kashyap,* and *Komal Prasad* for their cheerful company and extended help throughout the period.

I would also like to thank my past school and college teachers who were unparallel in their teaching.

I would like to specially thank *Ms. Mimi Mukherjee* and other friends *Mr. Sayan Santra, Mr. Rajkumar Jana, Ms. Mahima Makkar,* and seniors *Ms.Urmimala Maitra, Ms. Nabadyuti Barman, Ms. Moumita Rana, Mr. Ritesh Halder, Mr. Arpan De, Mr. Saikat Chakraborty, Mr. Jiarul Midya, Mr. Sisir Maity, Mr. Subhajit Paul, Mr. Koushik Pal, Mr. Anirban Mandol, Dr. Suman Majumdar, Dr. Pralok Kumar Samanta* who have been source of positive energy in all situation.

Above all, I would like to thank my grandparents, parents, and my relatives for all the love, affection and support to my research work.

Preface

In this thesis we report our study on characteristics of compounds with transition metal Cobalt and Chromium having unique oxidation state nature. Transition metals owing to their characteristic oxidation states and spin state transition alter various different properties like optical, catalytic, magnetic, and electrical etc. The thesis is focused on synthesis and characterization of one compound with transition metal at unusually high oxidation state and another one having transitional metal with unique spin state transitional nature

Chapter 1 deals with introduction of rare earth transition metal oxides, the synthetic routes which are followed, different possible crystal structure that they crystallize in and interesting applications of them.

Chapter 2 deals with the basic principles of various synthesis and characterization that have been taken help of during the course of study. The applicability of the techniques their limitations both in general and in our case have been discussed.

Chapter 3 depicts the synthesis and characterization leading to discovery of a new photocatalytic material of d^0 electronic configuration Lanthanum oxychromate (La_2CrO_6) that is capable of generation of H_2 from water. The approach towards detailed characterization and the applicability of this already known material is of prime focus here.

Chapter 4 explains the synthesis, magnetic and electrical protperties of $YCoO_3$ where the oxygen deficient sites alter the spin state transition of Cobalt in Yttrium cobalt oxide ($YCoO_3$) and thereby physical properties are altered.

Contents

Chapter 1

Introduction

Transition metal oxides construct one of the most interesting classes of inorganic solid materials via manifestation of wide range of structures, properties and their interesting applications. The intriguing properties that stay at the heart of this class of materials are basically the result of altercation of outer *d* electrons resulting in different type of bond formation. The lanthanides on the other hand are characterized by gradual filling of 4*f* subshell. The combination of these two classes has produced lots of tertiary and quaternary compounds which are very much fascinating in terms of crystal structure, band structure, different physical and chemical properties etc. As a result, in terms of applicability, these materials have found place at the different industries in the form of catalysts converting harmful chemicals to natural precursors or generating energy from regular common materials, at electrical industries in form of conducting or dielectric materials, as electrode materials of many day to day electrochemical devices. The structural aspect of these oxides is very much diverse. Crystals with complicated structure like well celebrated perovskites, hexagonal ferrites, pyrochlores, spinels, lamellar etc. have been seen. In terms of electrical properties, on one hand numerous electrically insulating oxides can be found and on the other hand metallic oxides have established their concrete place. One more striking feature that has put a feather to the electrical diversity is superconductivity. Recent rare earth transition metal super conductors have been proven to be of much higher critical temperature (T_c).The electronic properties originating from charge density waves, charge ordering, defect ordering are very intriguing. In terms of magnetic properties, these tertiary/quaternary oxides are very much

diverse, with so many different types of magnetic oxides being present *e.g.* NiO, $LaCrO_3$ show antiferromagnetic nature while CrO_2, $La_{0.5}Sr_{0.5}MnO_3$ are known ferromagnets [1].

1.1.
Synthetic strategies:

Synthesis of rare earth transition metal oxides is very much versatile in terms of concepts and approaches and requires considerable synthetic ingenuity. Sound understanding on principles of thermodynamics, phase equilibrium, kinetics is required to carry out a proper rational synthesis [2]. The wide variety of techniques that can be used to make these oxides has provided researcher a wide scope of study and thus with time lots of new routes of synthesis have been found. On one side, the straight forward solid state route is there where samples are ground and heated to produce the target material. In order to prepare compounds at low temperature with high purity and definition, solution gelation method are taken help of. Then there are some methods that take the reaction condition to the extreme like high pressure synthesis, rapid quenching etc. Among these more interest has grown on low temperature chemical synthesis due to higher control on the product in terms of structure, phase purity, stoichiometry and applicability. Some of the important chemical techniques of present day are solid state route, sol-gel method, coprecipitation method, ion exchange method, electrochemical method, hydrothermal synthesis, combustion method [3-9].

1.1.1 Solid state synthesis:

Most common method is obviously solid state synthesis known as ceramic route that includes thorough grinding followed by heating at suitable temperatures in desired atmosphere. Small yet effective modifications are often made like heating in the form of pressed pellet, intermediate grinding and heating. Platinum, silica or alumina boats are used as reaction vessel as they do not interact and are stable at high temperature. Sometimes the

constituents chosen are found volatile or the reaction to be carried out seems sensitive. For these cases heating in evacuated sealed tube is considered. This techniques are mainly applied for cation substitution reactions *e.g.* substitution of La^{3+} by Sr^{2+} in $LaCoO_3$, or substitution of La^{3+} by Ca^{2+} in $LaMnO_3$ etc. [10-11]. The main parameters that have to be satisfied for this kind of substitution are relative size and charge neutrality of the cations. Gopalakrishnan *et al.* substituted Ti by pentavalent Nb and proportionally replaced P by Si thereby preparing $KTi_{0.5}Nb_{0.5}OP_{0.5}Si_{0.5}O_4$ [12]. Present day sees this kind of substitution in rare earth cobaltites, chromites, manganites to very much extent. A very interesting variant of solid state route is combustion method. This is nothing but synthesis of complex oxides by decomposition of compound precursors. Various ternary or quaternary oxides are prepared by this method. Sometimes the reactivity is controlled by the crystal structure rather than the chemical nature. This type of solid state reactions are known as topochemically controlled reactions *e.g.* controlled reduction of $LaNiO_3$ or $LaCoO_3$ results in formation of $La_2Ni_2O_5$ and $La_2Co_2O_5$ respectively [11].

1.1.2 Ion exchange method:

Ion exchange method is another very frequently applied method. This method results in formation of layered [12], tunnel, close-packed structures. The reference data being too scattered, the basic concepts that formulate the nature of the reaction pathways and the product could not be ascertained yet. Still the method has found lot of interest due to applicability in preparation of metastable phases. For instance, reactions of $Ca_2CuO_2Cl_2$ or $Sr_2CuO_2Cl_2$ with $NaLaTiO_4$ lead to different interesting products [13]. Reaction of $KLaNb_2O_7$ with $FeCl_2$ leads to $FeClLaNb_2O_7$ [14].

1.1.3 Sol-Gel synthesis:

The second most common technique that is used is solution – gelation method. This is basically a wet chemical multistep process that has wide range of phenomena occurring under

its belt. Some are like complexation, polymerization, densification, drying etc. Sol-Gel is the name given to it because of the distinctive change is viscosity at a particular step of the reaction which is indicative of gel formation. The technique is applied when particles of submicrometre size and of narrow particle size distribution is required. Numerous types of compounds have thus been prepared by this method to date.

1.1.4 High pressure synthesis:

Use of high pressures to synthesize different compounds is well known technique nowadays. This method is applied to prepare compounds with elements at high oxidation state or compounds with energetically unfavourable phase to achieve. For relative low pressure criteria (1-10 kbar), hydrothermal synthesis is taken help of. Solid state syntheses are basically carried out with applied pressure in the range of 10 – 150 kbar. Rare earth orthoaluminates are very much known compounds which are prepared by this technique [15] while preparation of Iron based arsenic oxide superconductors are another type of example [16-17].

Use of alkaline medium in the form of either solid or molten fluxes is very much common and has produced lots of different compounds. The oxidizing atmosphere created by alkali fluxes influences the oxidation states of the materials. A good example of this kind of reaction is preparation of superconducting $La_2CuO_{4+\delta}$ by reacting mixture of La_2O_3 and CuO in molten KOH / NaOH around 520 K [18].

1.2.
Oxidation states of 3*d* transition metals:

The 3*d* orbitals of the first row transition metals stay partially or fully occupied with electrons. This gives rise to several possible oxidation states of the elements. The stability of

a given oxidation state depends upon several factors like nature of the element with which the transition metal is bonded, nature of ligand etc. Among 3*d* transition metals the highest oxidation state that is possible is +7 which is seen for Mn ($KMnO_4$). Mostly the electronegativity of the bonded element influences the oxidation state of the corresponding transition metal. The main possible oxidation states are shown below in table 1.1.,

Table 1.1 [19].

Elements	Sc	Ti	V	Cr	Mn	Fe	Co	Ni	Cu
Oxidation States	**3**	(2) **3** **4**	2 3 **4** 5	2 **3** (4)§ (5)§ 6	**2** (3) **4** (5)§ (6)§ 7	**2** **3** (4) (5) (6)	2 **3** (4) (5)	**2** (3) (4)	1 **2** (3) 4

Table 1.1. Main oxidation states of 3*d* transition metals. Most stable are shown is bold type while unstable are shown in parentheses. § indicates disproportionation.

Thus scandium (Sc) is having single common positive oxidation state III corresponding to ionization of both the 3*d* and 4*s* electrons. The immediate next oxidation state in terms of abundance is 2+. This is the result of 4*s* electron ionization only. The 2+ oxidation state seems to be fairly stable for higher transition metals. This is due to strong reducing nature of lower ones like Ti, V, Cr. Chromium (electronic configuration $3d^5 4s^1$) is seen to be having 3+ as the most stable oxidation state which represents $3d^3 4s^0$ electronic configuration. Lots of oxides like Cr_2O_3, $LaCrO_3$ are very common example of this. Next higher oxidation state that is stable is 6+ state ($3d^0 4s^0$) 4+ and 5+ being very unstable. Although Cr^{6+} seems to be very much stable still the thermodynamic

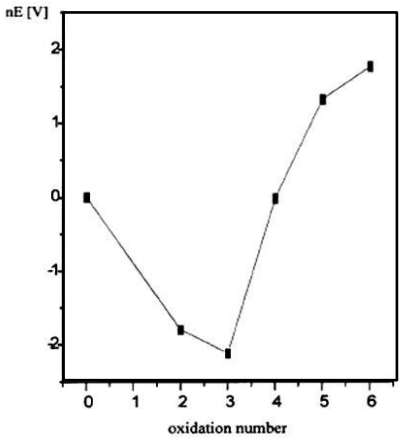

Figure 1.1. [20] Possible oxidation states of Cr.

feasibility of its reduction is not ignorable. The latimer diagram of Cr {c.f. Figure 1.1.} is indicative of this. In acidic medium Cr^{3+} is found to be more stable than Cr^{6+}:

$$HCrO_4^- + 7H^+ + 3e^- \underset{E: \pm 1.35\ V}{\rightleftharpoons} Cr^{3+} + 4H_2O$$

Thus in nature not many Cr(VI) compounds are found (CrO_3, $K_2Cr_2O_7$, oxohalides)and even the some of the existing materials are metastable (CrF_6). The cobalt on the other hand does not possess O.S. higher than 5+ although Co (V) is very much unstable, is likely to be present in materials having stoichiometry M_3CoO_4 which can be produced via heating in oxygen under pressure [19]. Co basically has two stable positive oxidation states 2 and 3 while Co^{3+} is found to be less stable compared to Co^{2+} in acidic medium.

The manganese (Mn) is the transition metal among the 3*d* series which shows maximum number of possible oxidation states as well as the highest oxidation state. In the table 1.1. it can be seen that on going from left to right the number of different oxidation states increases upto Mn and then decreases. This can be attributed to the variation in binding nature of 3*d* electrons.

1.3.
Structure:

Transition metals and rare earth oxides constitute of a large variety of crystals structures. The bonding between different transition metals and rare earth elements are very interesting and thus are very much subject of focus. Thus for proper understanding not only overall crystal structure and bonding is sufficient to know but also an insight about the local structures is required. These local structures at sub micrometre level often leads to various intriguing properties and are thus important to be studied. The different characterization techniques that are used at present are various and dependent on the aspect of the researcher. Though X-Ray and neutron diffraction techniques hold an integral part of the characterization

but there are other very much sensitive and important techniques also, electron microscopy, spectroscopic technique being some of them.

1.3.1 Perovskites:

Perovskite structures are the most common and well-studied in the family. Perovskites belong to a large class of compounds having crystal structures related to the mineral $CaTiO_3$. Ideally the crystal structure of cubic ABO_3 perovskite consists of corner sharing octahedra (BO_6). The A cation takes the 12-fold coordination site formed in the middle of the cube of eight such octahedra. The perovskite structures itself is very versatile and consists of different type of crystals like stoichiometric, nonstoichiometric oxygen deficient perovskites etc. Stoichiometric perovskites are of the general formula ABO_3 and their structure is based on ReO_3. Stoichiometric perovskites can be of many categories, the rare earth cation A and transition metals cation B oxides fall under type $A^{III}B^{III}O_3$ type. Ideally they should be cubic

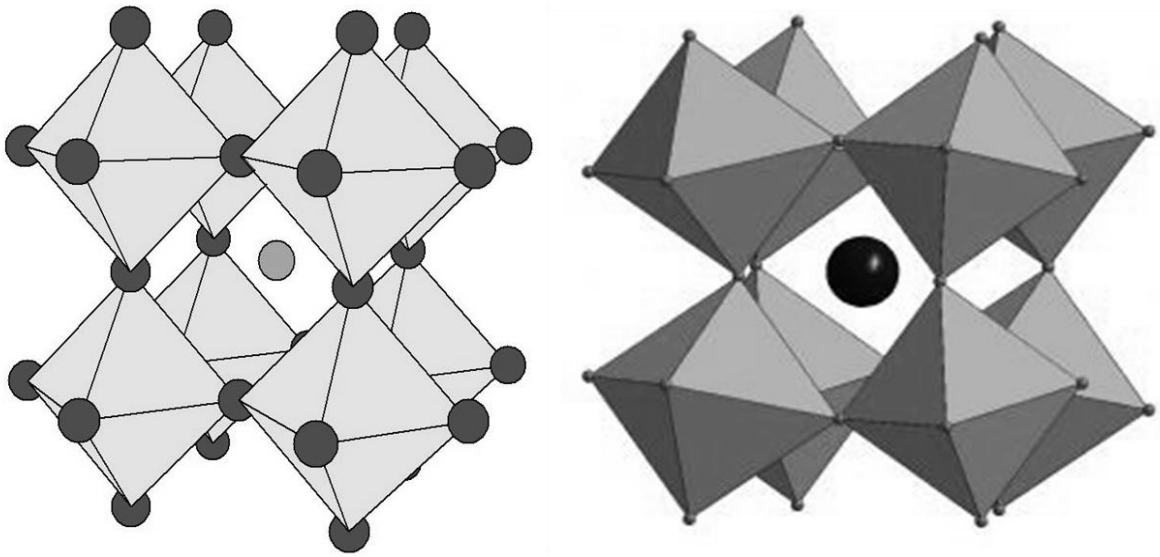

Figure 1.1.: Ideal cubic perovskite structure (left) distorted perovskite structure (right).

in symmetry but most of the ABO_3 perovskites exhibit distortion from this symmetry. This distortion often in turn generates interesting properties like ferroelectricity ($BaTiO_3$) in the material [21]. The $A^{III}B^{III}O_3$ are found to be distorted towards orthorhombic symmetry and in some extreme situation monoclinic structure has been seen *e.g.* $GdFeO_3$ (orthorhombic) [22],

$LnCoO_3$ (orthorhombic to monoclinic) [23]. In case of nonstoichiometric perovskites also the structure varies between cubic, orthorhombic and monoclinic. For instance Lanthanum bronze (La_xTiO_3) is seen to be crystallizing in cubic symmetry while in $Gd_x(Ta_{3n}W_{1-3x})O_3$ orthorhombic symmetry is observed [24]. The nonstoichiometric oxides have their important applications in insulator and dielectric material.

1.3.2 Pyrochlores:

The $Ln_2B_2O_7$ (Ln = Lanthanide, B = Ti, Zr etc.) series is seen to be having pyrochlore structure where the host lattice forms large cages resulting from intersecting tunnel [25-26]. For $Ln_2B_2O_7$ the host lattice is $(B_2O_6)_n$. The extra oxygens of the Ln_2O sublattice stay at the centre of the O_{18} cage. The Ln cations stay at the boundary between the two cages and thus these structures do not show any cationic mobility [24].

1.3.3 Garnets:

Garnets are oxides with mixed framework having the formula of $A_3B'_2B''_3O_{12}$. These structures are having 3-D host lattice ($B'_2B''_3O_{12}$) with corner sharing $B''O_6$ octahedra and $B'O_4$ tetrahedra. Each tetrahedron is linked to four octahedra while each octahedron os linked to six tetrahedral. Thus along <110> direction, alternating octahedra and tetrahedra form a row (c.f. figure 1.8) [24]. Numerous numbers of compounds are seen to be crystallizing in this structure. For instance, $Ln_nFe_5O_{12}$ (n = 2 for Dy; 3 for Gd, Sm, Nd, Eu, Tb, Ho etc.) [24].

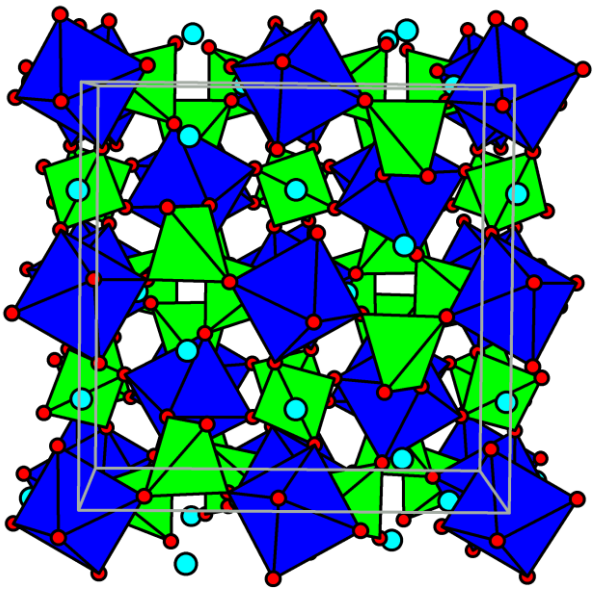

Figure 1.2. [27]: Typical garnet structure

1.3.4 Layered structures:

These are complicated mixed layered structures with stacking periods of up to 90 Å, stabilisation of unusual coordination polyhedral as 2 dimensional fragments. More complex variant of these structures is intermixed layers of different precursors. Sometimes structure may have superstructures or 2D ordering of perovskites also. Common examples are T-$[Ln_2O_2]CO_3$, $[Ln_2O_2]K_2(CO_3)_2$ etc. [12]. These structures are very much typical of the synthetic method of their preparation and have very unique properties which are mostly coming from layered nature.

1.3.5 Oxygen deficient perovskites:

Rare earth and transition metal quaternary compounds are also seen to be having oxygen deficient perovskite structure. 3-D framework structures with pyramidal octahedral mixed coordination construct one subgroup of these oxygen deficient compounds. For example, $BaLa_4Cu_5O_{13}$ consists of both CuO_5 pyramids as well as CuO_6 octahedra [28]. Due to 3-D nature of the frameworks these kinds of structures are often seen to be having strong magnetic interactions although instances of superconductivity are almost zero. The layered cuprates constitute one very celebrated class of compounds and thus is worthy to be mentioned. The orthorhombic perovskite $YBa_2Cu_3O_7$ has this type of structure where triple $[Cu_3O_7]_n$ layers of corner sharing polyhedral are seen [29]. Series of $La_xA_xCuO_4$ (A = Ca, Sr, Ba) is another very common example of this [30]. There are some materials which have perovskite structures inter grown with rock salt phase. These compounds have general formula as $(ABO_3)_m(AO)_n$ *e.g.* $(LaNiO_3)_n(LaO)$ where La_2NiO_4 is having K_2NiF_4 type structure and $LaNiO_3$ is perovskite [32]. The ability of Cu to adopt pyramidal, square planar coordination has led to the formation of a special subgroup of cuprates which have ordered

oxygen deficiency in a perovskite structure which is intergrown with rock salt layers. These materials have general formula of $(ABO_{3-x})_m(AO)_n$ *e.g.* $LaSrCaCu_2O_6$ [31].

1.3.6 Rare earth cobaltites:

3

Extensive investigations on rare earth cobaltites $LnCoO_3$ (Ln=Y or lanthanides) have been started from long back due to their characteristic structural features and unique magnetic and electronic transition which are related to changes in local spin states of Co^{3+} and the character of itinerant carriers [33-41]. In terms of crystal structure, the stoichiometric cobaltites do not fall under regular cubic perovskite structure characterized by $Pm\bar{3}m$ space group. $LaCoO_3$ crystallizes in rhombohedrally distorted cubic perovskite structure ($R\bar{3}c$) while other cobaltites of the series Ln = Pr to Lu and Y show an orthorhombic distortion of the perovskite cell characterized by the space group *Pbnm* (or the equivalent group *Pnma*). The decrease in Ln^{3+} cation radius results the transition of the perovskite structure from higher to lower symmetry. For example, $NdCoO_3$ shows a very small distortion and crystallizes in an almost cubic structure [9]. In all cobaltites, the cobalt ion is found to be surrounded by weakly distorted oxygen CoO_6 octahedra, whereas the rare-earth ions are in distorted cubo-octahedra formed of 12 oxygen ions (Figure 4.1.). Of the 12 Ln-O bonds, 3 are long, 6 are medium-length, and 3 are short bonds. This distortion effectively inverts b > a to a > b and in this fashion structural transition from orthorhombic to rhombohedral symmetry happens [23]. The magnitude of structural distortions changes significantly with the change in temperature also.

1.4.
Physical properties:

The diverse structures and the variety of properties exhibited by transition metal and rare earth oxides are very much rich in context. External physical parameters like

temperature, electric field, magnetic field, mechanical stress etc. act as external stimuli and have very much impact on the physical properties of the oxides.

1.4.1 Electronic properties:

Being a subclass of a broader series of 3*d* TM oxides, the TM and RE oxides form a congregation most of which have partially filled 3*d* bands and yet are magnetic insulators. Due to presence of strong on-site Coulomb repulsion in these insulators, a Coulomb gap is manifested in the partially filled narrow 3*d* band. The Coulomb repulsion is not mitigated by the restricted range of kinetic energies available to an arrow-band system. Among many different RE and TM oxides the most interesting feature is shown by those of cobalt. The hallmark of cobalt oxides which separates from other 3*d* metal oxides deals with the ability of cobalt to be present in various spin states, that is, low spin (LS), high spin (HS), and intermediate spin (IS) state. The theory behind this is very much complicated and has not been completely realised so far. The reason behind this complexity is the fact that the crystal field splitting Δ_{cf} of the 3d energy level of the cobalt ion in cobalt oxides is of the same order of magnitude as the Hund's rule intra-atomic exchange energy J_H and the 3d-orbital bandwidth which makes these different spin states very much possibility and abundant. Considering octahedral geometry the cobalt oxides have Co^{2+} always in high-spin state $t_{2g}^5e_g^2$ (S=3/2) as decided by Hund's rule while crystal field comes into effect in case of Co^{4+} which takes low-spin state $t_{2g}^5e_g^0$ (S=0). The Co^{3+} instead does not fall among the two mentioned above and shows low-spin $t_{2g}^6e_g^0$ (S=0), high-spin $t_{2g}^4e_g^2$ (S=2) and Intermediate-spin state $t_{2g}^5e_g^1$ (S=1). The reason being the ligand effect of O on Co atom and thus the Co-O bond length and Co-O-Co bond angle determine the spin state.

1.4.2 Magnetic properties:

The transition metal oxides show diamagnetic nature when in d^0 electronic configuration *e.g.* TiO_2, V_2O_5, ZrO_2, Nb_2O_5. The magnetic property changes towards

paramagnetism (pauli paramagnetism) for oxides having higher electronic configuration (d^n) *e.g.* TiO, NbO, V_2O_3, MoO_2 etc. One observable feature of first row transition metals is that the agreement between calculated and experimental moment is very poor. This agreement can be improved if the spin contribution is considered only. The lanthanide oxides on the other hand show paramagnetism and follow Curie-Weiss law. This paramagnetic nature is characteristic of f^n electrons as the experimental value of effective magnetic moment goes well with the ground state value. Sm and Eu show deviation from this common nature owing to presence of higher multiplets. When these two types of elements combine and form new structures, the overall band diagram and bonding changes drastically originating new features. Consequently magnetic property changes a lot. For several compounds of this category, often the adjacent atomic moments interact with each other. This correlation is strong is some cases and in some cases it is weak. Different mechanisms of this correlation process are there. The exchange process is one of them. For closed spaced atoms direct exchange occurs and for distant ones the exchange acts through intermediate nonmagnetic ions (superexchange) or itinerant electrons (RKKY interaction). $LaCrO_3$, $LaFeO_3$ are compounds where superexchange influences the magnetic ordering temperature [42].

1.4.2.1 Diamagnetism:

The diamagnetic nature as depicted above originates from absence of any unpaired electrons in uppermost shell. Thus the oxides having $5d^0 6s^0$ (for rare earth''s) and also $3d^0$ or (for transition metal's) electronic configuration show diamagnetic behaviour. Compounds with transition metal having $3d^n$ electronic configuration show diamagnetic nature provided the n no of electrons have to be spin paired.

1.4.2.2 Ferromagnetism:

Apart from these two noncooperative phenomena dia and paramagnetism, cooperative phenomenon like ferromagnetism is also seen for these oxides. With increase in external magnetic field, these materials are seen to be increasing their magnetic moment initially. Their magnetic domains of favourable orientation with respect to external magnetic field change respective sizes at the expense of other domains. At certain temperature due to excessive increase in thermal energy the ordering vanishes and the respective material becomes paramagnetic. $La_{0.5}Sr_{0.5}CoO_3$, $La_{0.5}Sr_{0.5}MnO_3$, nano and bulk $LaCoO_3$ are very common examples of ferromagnetic oxide materials [43-46].

1.4.2.3 Antiferromagnetism:

Antiferromagnetism is also a cooperative phenomenon and is characterized by long range ordering of identical spontaneous moments. Due to negative exchange parameter value, the adjacent moments are opposite and thus below T_N these types of materials can be seen as interpenetrating sublattices of opposite moment value. $LaCrO_3$ shows antiferromagnetic behaviour below 320 K [47]. Some rare earth oxides of manganese show antiferromagnetism. Certain antiferromagnetic oxides show a unique magnetic nature of nonzero magnetic moment in absence of external magnetic field owing to canting of multiple antiferromagnetic lattices at an angle. These are called as canted antiferromagnets (CAFM) or weak ferromagnets. For example, $YCrO_3$ is a canted antiferromagnet [48]. The rare earth chromites $LnCrO_3$ (Ln = La, Nd etc.) were initially considered to be antiferromagnetic in nature. Further magnetic measurements at low temperatures have revealed them to be of CAFM type [48].

1.4.2.4 Spin glass:

Another very important type magnetic response is found for some materials which is

known as spin glass behaviour. The rare earth transition metal pyrochlores ($Ln_2Ti_2O_7$) exhibit this kind of behaviour [49]. The phenomenon is nothing but freezing of magnetic moments in random orientations. It is a disordered magnet with frustrated interactions intensified by stochastic positions of the spins where conflicting interactions are randomly distributed. The term "glass" represents the comparability of magnetic disorder with conventional positional disorder of glass.

1.4.3 Electrical Properties:

The electrical properties of these materials oscillate from insulating materials to superconductors, from dielectrics to fuel cell materials. The vast array of oxides truly offers a complete package to the scientific society. Although the overall nature of the different oxide materials is of semiconductor type, the variation is sometimes gigantic and thus worthy to elaborate to some extent.

The rare earth manganites are very much illuminated in this picture due to their plethora of properties coming from not electrical or magnetic property individually but also due to the interplay between them. For instance, $TbMnO_3$ is a compound in this class which is having antiferromagnetic ordering (below 41 K) as well as ferroelectric properties (below 28 K) and thus, is a concrete example of this scenario [50]. $LaMnO_3$ is the parent compound of this series of compounds which show colossal magnetoresistance and have layered antiferromagnetic ordering. The manganite $PrMnO_3$ is an antiferromagnetic insulator. Now in the compound, when in this structure Mn is doped with Fe, the resulting double perovskite Pr_2MnFeO_6 results in modified tolerance factor. As a consequence of that, the new material shows ferromagnetic insulator type nature [51]. Among doped manganites, the best studied system is a Mn^{3+}/Mn^{4+} system with formula $La_{1-x}A_xMn_{1-x}Mn_xO_3$ (A = Ca, Sr, Ba, or Pb) which for $0.17 < x < 0.4$ become ferromagnetic in nature and exhibit an insulator - metal (I - M) transition [52]. In summary, the variety of bulk as well as local magnetoelectric effects

are observed in $RMnO_3$ compounds with $R = Sc, Y, In, Ho, Er, Tm, Yb$ etc. are because of the coexistence of ferroelectric and magnetic ordering. On one side, magnetoelectric properties are seen on a large scale. On the other hand, the domain wall interaction leads to a coupling of ferroelectric and antiferromagnetic domains.

Rare earth chromites also have magnetic and electrical properties interacting in harmony. The heavier chromites ($LnCrO_3$ with Ln = Ho, Er, Yb and Lu) show frequency dependent dielectric constants indicating them to be relaxor ferroelectric although the lower end chromites ($LaCrO_3$, $NdCrO_3$) do not show similar nature [48].

The cobalt oxides are the most fascinating class of materials among the series owing to the spin state transition of Co. Divalent Co^{2+} ion always stay in high-spin state. At this state a high spin electron is easily localized on the site forming a small polaron. For an electron located on Co^{2+} to hop to the high-spin Co^{3+} the energy window that has to be overcome cannot be matched because of the small transfer energy of the t_{2g} bands. Owing to large spin flip requirement condition (from S = 3/2 to S = 0) it also cannot hop to a Co^{3+} ion in the low-spin state. This makes the Co^{2+} oxides act as magnetic insulators [23]. The oxides with intermediate valence between Co^{2+} and Co^{3+} has different situation. In these materials the carriers are often confined to the Co^{2+} sites thus making a mixed Co^{2+} / Co^{3+} system sensitive for charge segregation and charge and/or spin ordering. Consequently, the cobalt oxides having a cobalt valence state in between 3+ and 2+ often exhibit large dielectric constants [23]. On the other hand, Co^{4+} in the low-spin state is chemically much less stable. The oxygen ligand hole is likely to exist in the Co^{4+} system. The ligand hole tends to be itinerant and ferromagnetic metallic compounds are often realized in the intermediate valence between Co^{3+} and Co^{4+} [23]. Another interesting feature of the Co^{4+} valence state is the large entropy associated with the hole in t_{2g} level that causes huge thermopower. Thus, thermoelectric cobalt oxides can be realized in systems with cobalt valences intermediate between Co^{3+} and

Co^{4+} [23]. $LaCoO_3$ shows insulator to metal transition at 540 K where effective magnetic moment derived from susceptibility measurement concluded that the room temperature semiconducting nature is due to Co^{3+} ions at intermediate spin state while the high temperature metallic state is due to mixed spin state [53]. The other cobaltites in this series also show similar nature. The low temperature conduction of these cobaltites is associated with extra carriers present because of weak nonstoichiometry. In general the carriers are of hole type. Now at higher temperature the hole concentration increases considerably thereby increasing the conductivity. People have tried to control the hole concentration at low temperature by carrying out slight substitution of La ions by divalent metal ions like Ca, Sr, Mg etc. These doped compounds showed I – M transitions at much lower temperature than the mother compound [54].

Superconductivity: Superconductivity in oxide systems was discovered first in La/Ba/Cu/O systems by Bednorz and Muller in 1986 [55]. Since then, numerous number of superconducting oxide materials have been discovered. The cuprates form integral part of it, $La_{2-x}Ba_x(Sr_x)CuO_4$ being one of them. It is having characteristic T_c at 35 K [24]. Other oxide materials include $La_2CuO_{4+\delta}$ (T_c 39 K), $La_2Ca_{1-x}Sr_xCu_2O_6$ (T_c 60 K), $TlSr_2Y_{0.5}Ca_{0.5}Cu_2O_7$ (T_c 90 K) etc. [24].

1.4.4 Photocatalysis:

Present days see heterogeneous photocatalysis as a very important field of interest and concern due to very vast areas of environmental impacts. Different mechanisms of catalysis and their characteristic applicabilities are very much in focus and under the radar of constant development. Increased global temperature, diminishing energy sources and many other adverse effects have forced mankind to take efficient measures to reduce it and in this order the potential of heterogeneous photocatalysis have surfaced. Decomposition of harmful chemicals to biodegradable derivatives, production of energy from naturally available sources

are at present having very high impact in the scientific and industrial society and thus scientists are leaving no stone unturned to find proper material in terms of efficiency and versatility. The semiconductor heterogeneous photocatalysis has claimed huge focus as a emerging solution for both energy crisis and environmental hazards. It was first discovered by Fujishima and Honda [56]. They showed that water can be photo-electrochemically decomposed into constituent elements hydrogen and oxygen using a semiconductor (TiO_2) electrode under UV irradiation. Since then, keeping energy concern in mind, extensive works have been carried out to produce hydrogen from water splitting using a variety of semiconductor photocatalysts. Semiconductor photocatalysts on exposure to light beam of energy equal or greater than the band gap energy generates electron-hole pairs due to bandgap excitation and thus hole is created at valence and while electron goes from valence to conduction band. So electron – hole pair gets created as depicted in the expression below:

$$\text{Photocatalyst} \xrightarrow{h\upsilon} e^{-}(CB) + h^{+}(VB)$$

The excited electron-hole pairs then can either recombine very easily, releasing the absorbed energy as heat or can move and further react. If the electrons (and holes) migrate to the surface of the semiconductor without recombination, then these can actively participate in various oxidation and reduction reactions with various adsorbed chemicals such as water, methanol, other alcohols etc. The hole being an oxidant can oxidize different polluting organic and inorganic materials easily. In case of water splitting, the hole interacts with hydroxide ion (OH^-) to generate OH● radicals. These radicals can further covert into

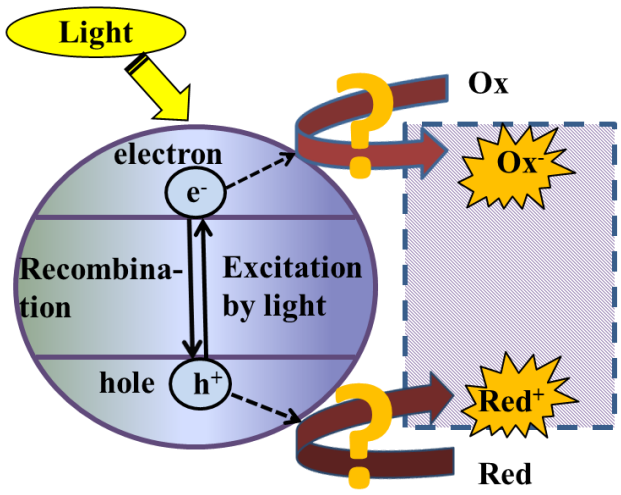

Figure 1.3.: Photocatalysis diagram.

oxygen. In order to generate oxygen the valence band position thus has to be more positive than oxygen production level. On the other hand the electrons on the conduction band are very much important when one considers hydrogen evolution phenomenon. The water dissociates as:

1. $2H_2O \rightarrow 2H_2 + O_2$
2. $H_2O \leftrightarrow H^+ + OH^-$
3. $2H_2O + 2e^- \rightarrow H_2 + 2OH^-$
4. $2H_2O \rightarrow O_2 + 4H^+ + 4e^-$

The reaction (1) is associated with a redox potential change of -1.23 V at pH 7. The half reactions (3) and (4) have redox potentials of -0.41 V and 0.82 V respectively [57]. Now for evolution of hydrogen, the conduction band position has to be more negative than hydrogen redox potential.

The degradation of polluting organic or inorganic compounds also proceeds via oxidation or reduction of the material and thus follows the same concept. Methylene blue, methyl orange, rhodamine B (Rh.B), phenol are some of the common organic pollutants. Among rare earth elements La, Ce, Pr, Nd and Sm are found to be constituent of different oxide and nitride materials that act as photocatalysts [58]. Apart from La, all other elements construct d^0 system photocatalyst oxides. These d^0 oxide systems are found to be having conduction bands composed of *d* and *sp* orbitals and valence band composed of O 2*p* orbitals. For nitrides N 2*p* orbitals constitute the valence band. There are number of perovskite oxides and oxynitrides in the list which can act as catalyst in presence of light. For instances, La_2TiO_7, $La_2Ti_2O_7$:Ba, $KLaZr_{0.3}Ti_{0.7}O_4$ are some examples of layered perovskite structures that exhibit high quantum yield values [59-60]. The reason behind the layered perovskite's catalytic activity is high cationic charge and the optimum layer thickness [57]. The cubic

pyrochlore structures are also phtocatalytically active *e.g.* $Ln_2Ti_2O_7$ (Ln = Gd, Y) [65-68]. All the above mentioned compounds are d^0 systems. Some d^{10} oxide systems are $LaInO_3$, $Y_xIn_{2-x}O_3$ [61-62]. These d^0 and d^{10} systems show hydrogen evolution on exposure to UV light not visible radiation. There are oxide materials which do evolve H_2 under visible light radiation as well *e.g.* $La_2Ti_2O_7$:M (M = Cr, Fe) [63-64].

1.5.

Motivation:

The thesis work is motivated towards synthesis, characterization and potential applicability of a new rare earth transition metal oxide La_2CrO_6 as well as synthesis of $YCoO_3$, creation of oxygen deficiency in the compound and its characteristic effects on electrical and magnetic properties. Being a d^0 system, it has fair chance of showing interesting electrical and catalytic properties. On the other hand deficiency in oxygen stoichiometry can alter the spin state population of cobalt and even the oxidation state also. These effects further can alter the characteristic magnetic and electrical transitions of $YCoO_3$.

1.6.

Bibliography:

1. Roy, R.; Solid State Ionics **1989**, 3, 32.
2. Rao, C. N. R.; Gopalakrishnan, J; New Directions in Solid State Chemistry; Cambridge University Press, Cambridge, 1986.
3. Soft Chemistry Routes to New Materials: Proceedings of the International Symposium, Nantes, 1993, Trans Tech Publications, Switzerland.

4. Hagenmuller, P.; Preparative Solid State Chemistry; Academic Press; New York; 1972.
5. Hoing, M. J.; Rao, C. N. R.; Preparation and Characterization of Materials; Academic Press.
6. Corbett, D, J; Solid State Chemistry – Techniques; Clarendon Press; Oxford; 1987.
7. Salvo, Di, J, F; Science **1990**, 247, 647.
8. Rao, C. N.R.; Chemical Approaches to the Synthesis of Inorganic Materials; Wiley; New York; 1994.
9. Goodenough, B., J.; Prog. Solid State Chemistry **1987**, 5, 149.
10. Rao, C. N. R.*et al.;* J. Solid State Chem. **1977**, 27**,** 353.
11. Vidyasagar, K.; Reller, A.; Gopalakrishnan, J.; Rao, C. N. R.; J. Chem. Soc. Commun. **1986**, 336.
12. Charkin, O., Dimitri; Grischenko. O., Roman; Sadybekov, A., Arman; Goff, J., Richard; Lightfoot, Philip; Inorg. Chem. **2008**, 47, 3065.
13. Sivakumar, T.; Lofland, S. E.; Ramanujachary, K. V.; Ramesha, K.; Subbanna, G. N.; Gopalakrishnan, J.; J. Solid State Chem. **2004**, 177, 2635.
14. Kodenkandath, T. A. *et al.* Wiley, J. Inorg. Chem. **2002**, 41, 3385.
15. Dernier, P. D.; Maines R.G.; Materials Research Bulletin **1971**, 6, 433.
16. Ren Zhi-An *et al.*; Europhys Letters **2008**, 83, 17002.
17. Ren Zhi-An *et al.*; Chin. Phys. Lett. **2008**, 25, 2215.
18. Ham, W. K.; Holland G. F.; Stacy, A. M.; J. Am. Chem. Soc. **1988**, 110, 5214.
19. Sarkar, R; General and Inorganic Chemistry, 2007.
20. Shriver *et al.*; Inorganic Chemistry; 2nd edition 1994.
21. Jona, F.; Shirane, G.; Ferroelectric Crystals; Pergamon Press, New York, 1962.
22. Coppens, P. *et al.* Acta Crystallographica (1,1948-23,1967), (1965), 19, 524-531.

23. Raveau, Bernard; Seikh, Md. Motin; Cobalt Oxides: From Crystal Chemistry to Physics, First Edition. Wiley-VCH Verlag GmbH & Co. KGaA, 2012.

24. Rao, C. N. R.; Raveau, B.; Transition Metal Oxides, VCH Publishers, Inc., 1995.

25. Kimura, M. *et al.* Acta Crystallogr., Sect. B **1975**, 31, 1912.

26. Prasadarao, A. V. *et al.* A. S. Mater. Lett. **1991**, 12, 306.

27. http://chemistry.osu.edu/~woodward/ch754/struct/Ca3Fe2Si3.htm

28. Raveau, B. *et al.* Journal of Solid State Chemistry **1974**, 68,143-152.

29. Calestani, G.; Rizzoli, C.; Nature (London) **1987**, 328, 606-607.

30. Raveau *et al.*; Crystal Chemistry of High T_c Superconducting Copper Oxides; Springer-Verlag; Berlin; 1991.

31. Ganguly, P.; Rao, C. N. R.; J. Solid State Chem. **1984**, 53, 193.

32. Demazeau, G. *et al.*; J. Solid State Chem. **1974**, 9, 202.

33. Seikh M.M. and Raveau, B., Giant Magnetoresistance: New Research (eds Adrian D. Torres and Daniel A. Perez), NOVA Publishers, pp. 107, 2009.

34. Rao C.N.R. *et al.*; Top. Curr. Chem. **2004**, 234(II), 1.

35. Ivanova, B. N.; *et al.*; Physics-Uspekhi; **2009**, 52, 789.

36. Thornton, G. *et al.*; J. Solid State Chem. **1986**, 61, 301.

37. Raccah, P. M.; Goodenough, J. B.; Phys. Rev. **1967**, 155, 932.

38. Kappatsch, A. *et al.*; J. Phys. France **1970**, 31, 369.

39. Yakel, H. L.; Acta Crystallogr. **1955**, **8**, 394.

40. Wold A. and Ward R., J. Amer. Chem. Soc. **1954**, 76, 1029.

41. Zhou, J.-S. *et al.*; Phys. Rev. Lett. **2005**, 94, 06550.

42. Hearne, G. R. *et al.;* Physical Review B. **1995**, 51, 11495.

43. Roy, B.; Das, S.; Journal of Alloys and Compounds **2011**, 509; 5537.

44. Medvedeva, Julia E.; J. Phys.: Condens. Matter **2002**, 14**,** 4533.

45. Zhou *et al.*; Physical Review B.; **2007,** 76, 172407.

46. Yan, J,-Q *et al.*; Physical Review B. **2004**, 70, 014402.

47. Weinberg, I.; Larssen, P.; Nature **1961,** 192, 445.

48. Sahu, Jyoti, Ranjan *et al.*, J. Mater. Chem. **2007**, 17, 42.

49. Greedan, John E,; Journal of Alloys and Compounds **2006**, 444, 408-412.

50. Kenzelmann, M.; Physical Review Lett. **2005**, 95, 087206.

51. Ganeshraj, C. *et al.*; Journal of Applied Physics **2010**, 107, 09E305.

52. Jirak, Z.; Hejtmanek, J.; Knizek, K.; Journal of Solid State Chemistry **1997,** 132, 98.

53. Heikes, R *et al.*; Physica (Amsterdam), **1964**, 30, 1600.

54. Jirak, Z.; Physical Review B. **2008**, 78, 014432.

55. Bednorz, J. G.; Muller, K. A.; Z. Phys. **1986**, B64, 187.

56. Fujishima. A; Honda, K. Nature **1972**, 238, 37.

57. Kudo, A.; Kato, H.; Tsuji, I. Chem. Lett. **2004**, 33, 1534.

58. Kudo, A.; Miseki, Yugo; Chem. Soc. Rev. **2009**, 38, 253.

59. Kim, J.; Top. Catal. **2005**, 35, 295.

60. Reddy, V. R.; Hwang, D. W.; Lee, J. S.; Catal. Lett. **2003**, 90, 39.

61. Sato, J.; Saito, N.; Nishiyama H.; Inoue, Y.; J. Phys. Chem. B, **2003**, 107, 7965.

62. Arai, N. *et al.* J. Phys. Chem. C **2008**, 112, 5000.

63. Hwang, D. W. *et al.* Catal. Today **2004**, 93, 845.

64. Hwang, D. W. *et al.* J. Phys. Chem. B **2005**, 109, 2093.

Chapter 2

Experimental techniques

2.1
Synthetic strategy:

Solid materials can be synthesized via numerous techniques; the appropriate method is adopted depending on the criteria of the experimentalist like expecting certain form of the product. The form can be amorphous or crystalline or mixture of both. Again these materials can be in the form of single crystal, poly crystals or thin film. Herein two very well-known methods have been considered. They are solid state synthesis and sol-gel synthesis. Though considerably different, these two often go hand in hand in order to produce modern day materials with good characteristic properties.

2.1.1 Solid state synthesis:

Standing on the concept of thermal diffusion this is the most straight-forward and most widely used method for preparation of polycrystalline solids. In this method, the reactants in the form of solids are ground together very well to make sure that these are finely crust and intermixed properly. Then the mixture is heated at suitable high temperature for specific hours of time in order to get desired product. Thermal diffusion occurs at the interface of two different reactants. At first

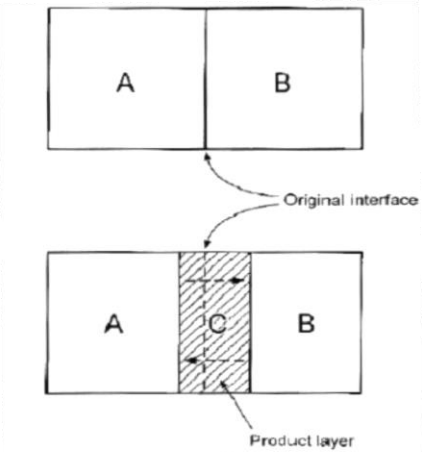

Figure 2.1.: Solid state diffusion

nucleation occurs which further leads to agglomeration and increase in the product layer length {c.f. figure 2.1.}. The solids if mixed and kept at room temperature, do not go diffusion very easily and thus product is not formed at all. The reason behind this is structural mismatch between the reactants and the product which creates an energy barrier. For diffusion and nucleation to occur, bonds must be broken and reform and then only atoms can migrate through interface. This needs external energy. At higher temperature the external energy comes in the form of heat and takes the reaction forward. The heating temperature is considered as optimum when at 2/3 of the melting point of the reactants. The diffusion process is very slow. Powder of average particle size in the range of nm-μm is favoured for proper diffusion to occur and thus the mixture is ground properly before heating. In some cases powder is successively ground and heated in a cycle in order to make sufficient diffusion to occur and thereby drive the reaction forward. Another very popular way to increase diffusion is to make pellet of the power by compression and then heating it. In this way the diffusion length can be decreased much. Thus void spaces can be avoided and reaction becomes much more accurate. The reactants, in the form of pellet or powder can be heated in oxidizing or reducing or even inert atmosphere which can be created in situ as per the criteria. Solid state method can be applied in various cases like, preparation of numerous compounds at various conditions, for removing moisture or adsorbed gases, modifying pre-synthesized compounds, influencing structural transition etc.

In present study we have used this technique in various cases. In order to remove adsorbed CO and moisture, La_2O_3 was heated at 900 °C for 12 hours in presence of atmospheric air in a box furnace. Further the La_2CrO_6 and $YCoO_3$ precursors which were got after sol gel synthesis were heated at 550-800 °C and 920 °C respectively in oxygen flow to oxidize and drive off all the carbon present. For electrical and magnetic measurement purpose well sintered dense pellets were required. These were made by heating respective

compounds in the form of pellet at optimum temperature in oxygen flow. La_2CrO_6 was heated at 800 °C and that of $YCoO_3$ was heated at 920 °C.

2.1.2 Sol-Gel synthesis:

Solution Gelation method is based on dissolution of the reactants followed by distinguishable sharp change in viscosity indicating formation of gel type precursor via heating at low temperature (100-250 °C). The most basic aspect of this method that makes it much different from the solid state method is that all the reactants are dissolved in solvent and thereby a solution is produced. Now obviously this is very much homogeneous when compared to the solid state reactant mixture prior to heating, even if well ground. The result of this is product purity is very high. As low heating temperature is required, the compounds which are having low melting points or structurally unstable at high temperature can be used in or synthesized using this technique. Thus the method is suitable for mixed salts like carbonates, sulphates, chromates, cobaltites etc. and particularly for hygroscopic phases. There are two types of Sol-Gel techniques, polymeric and colloidal. In the polymeric sol-gel technique the gel forms due to polymerisation while in colloidal method electrostatic repulsion is the reason behind gel formation. Both the techniques are dependent on few factors like reactant/solvent ratio, reactant/fuel ratio, pH of the solution, fuel's flash point temperature, duration of reaction etc. Thus in short although relatively complex to understand when compared to solid state, the sol-gel technique leads to synthesis of particles which are of very clean phase and definite homogeneity.

Here we have prepared La_2CrO_6 and $YCoO_3$ precursor via citrate sol-gel technique in acid medium. Preheated La_2O_3 and Y_2O_3 were taken along with nitrate salts of Cr and Co respectively. Citric acid was added as complexing agent as well as fuel. Final heating temperature of the gel precursor was 200 °C (flash point of citric acid is 200 °C) whereby

final product precursor along with amorphous carbon was obtained. This precursor was then heated at optimum temperature for suitable duration in order to get the pure phase products. The optimum temperatures were 800 °C for La_2CrO_6 and 920 °C for $YCoO_3$.

2.2

X-ray diffraction pattern and Rietveld Refinement:

X-ray diffraction is a tool for the investigation of the fine structure of materials. The technique was invented since 1912 when von Laue had discovered diffraction of x-rays by crystals, which can be used to reveal the crystal structure. At first, x-ray diffraction was used only for the determination of crystal structure. Later on, other uses like measurement of particle size, chemical analysis, stress measurement, phase equilibria study, orientation of crystals have been developed.

A crystal structure is determined from a good quality X-ray diffraction pattern. The peak shapes in the X-ray diffraction data is a combination of Gaussian and Lorentzian functions. For highly symmetric crystals, the diffraction pattern consists of well-defined and well resolved intense peaks. This pattern can be called as good one and is sufficient for refining to get all the information about the crystal structure with good accuracy. So-called refinement is nothing but the method of obtaining real structural parameters from powder diffraction pattern. It was first proposed by Reitveld for powder neutron diffraction data and was applied for the nuclear and magnetic refinement [1, 2]. Further, X-ray diffraction was also included. The method is based on the least square of the difference of observed and calculated pattern. The pattern refinement method is used to fit a calculated profile pattern to observed powder diffraction data. In this process both structural and instrumental parameters get refined but this is not global minimum. The global minimum is achieved by the application of Rietveld refinement method which requires information about space group,

approximate lattice parameters and atomic positions and instrumental parameters like X-ray wavelength etc. prior to application. For the observed intensities of scattered radiation being y_i for i^{th} data point (i denoting 2θ increment) in the powder diffraction pattern, and calculated intensity being y_{ci}, the relation between them will be the following:

$$y_{c1} = ky_1$$

$$y_{c2} = ky_2$$

$$y_{c3} = ky_3$$

……

$$y_{cn} = ky_n$$

Non-linear least-squares refinement is applied in order to solve the above system of equations which aims to minimize the sum of the residual over all data points. The residual least square (S_y) is given by,

$$S_y = \sum_{i=1}^{n} w_i (y_i - y_{ci})^2$$

The fitting quality of a Rietveld refinement can be examined by a difference plot of the calculated and observed profile patterns. Ideally this should be a straight line. There are several figure of merit to see the goodness of the refinement.The weighted profile residual (R_{wp}), and the expected profile residual (R_{exp}) have been used here. These are given by,

$$R_{wp} = \left[\frac{\sum_{i=1}^{n} w_i (y_i - y_{ci})^2}{\sum_{i=1}^{n} w_i (y_i)^2}\right]^{\frac{1}{2}}$$

$$R_{exp} = \left[\frac{n-p}{\sum_{i=1}^{n} w_i (y_i)^2}\right]^{\frac{1}{2}}$$

The goodness of fit (x^2) is given by:

$$\chi^2 = \frac{\sum_{i=1}^{n} w_i (y_i - y_{ci})^2}{n-p} = \left[\frac{R_{wp}}{R_{exp}}\right]^2$$

This value should ideally be 1 but in practice it varies in the range of 1.1 - 1.8 for fitness of a profile that is considered as good [3]. The X-ray diffraction patterns, reported here, were recorded in Bruker D8 Advance Diffractometer and PANalytical Empyrean single wavelength ($K_{\alpha 1}$) diffractometer. All the data were plotted using standard softwares and in order to calculate grain size peak fitting was carried out in voight profile fitting method.

2.3 Magnetic measurement:

When a material is placed within a magnetic field, the magnetic forces of the material's electrons will be affected. Based on the overall electronic magnetic force response materials can interact quite differently with external applied magnetic field. This interaction is dependent on a number of factors, such as the atomic and molecular structure of the material, and the net magnetic field associated with the atoms. The magnetic moments associated with atoms have three origins. These are the electron motion, the change in motion caused by an external magnetic field, and the spin of the electrons. Accordingly different classes of magnetic materials have been surfaced e.g. Diamagnetic, Paramagnetic, Ferromagnetic, Antiferromagnetic, Ferrimagnetic materials. Diamagnetic materials have a weak, negative susceptibility to magnetic field; these materials are slightly repelled by a magnetic field and do not retain the magnetic property when the external field is removed. In these materials all the electrons are paired so there is no permanent net magnetic moment per atom. Paramagnetic materials have a small, positive susceptibility to magnetic field. These are slightly attracted by a magnetic field and the material does not retain the magnetic properties on removal of the external field. Presence of some unpaired electrons and realignment of the electron paths caused by the external magnetic field creates this property. Ferromagnetic materials have a large, positive susceptibility to an external magnetic field. They exhibit a strong attraction to magnetic fields and are able to retain their magnetic

properties after the external field has been removed. They get their strong magnetic properties from the collective effect of magnetic domains. Antiferromagnetic materials have non zero magnetization to an external field. These materials have alternating spin structure of same moment value and thus show no magnetization when external field is removed. They should have had zero net magnetization in nonzero external magnetic field also but due to canted spins the small magnetization is observed. Ferrimagnetic materials also have alternating spin structure but the opposite spins are of different moments. Proper magnetic measurements lead to characterization and understanding on these materials and thus are very important technique to use.

2.3.1 SQUID Magnetometer:

A SQUID Magnetometer of the type Quantum Design MPMS - VSM is built with a helium cryostat and superconducting magnet. A schematic diagram is given in fig 2.2.

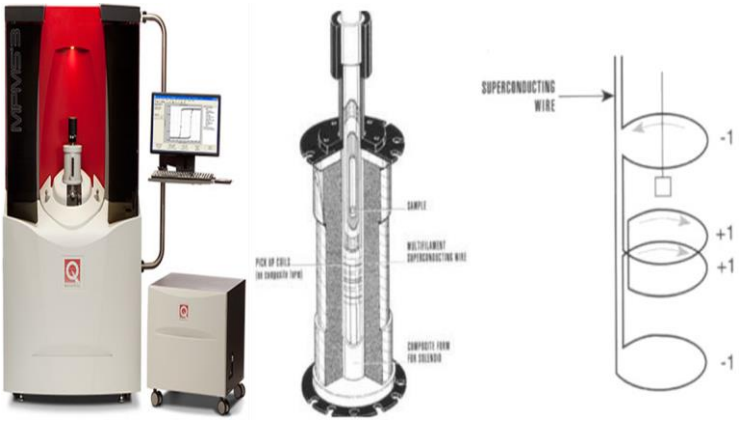

Figure 2.2. SQUID VSM

The helium gas controls the sample temperature. The SQUID detector is a Josephson contact loop which is placed at the core of the apparatus. This is exposed to the field of superconducting magnet and gradually moved through a pick-up coil system. The pick-up coil system is an arrangement of induction coil where the upper and lower single turns are counter wound with respect to the two-turn center coil [4]. This arrangement rejects interference from nearby magnetic sources. The sample

magnetization induces a voltage when it vibrates through the coil according to the Faraday's law. The SQUID detector measures this induced voltage and change it to the magnetization by software. If the oscillation of the sample is sinusoidal then the induced voltage (V_{coil}) is given by,

$$V_{coil} = 2\pi fCmA\sin(2\pi ft)$$

Where f and A are the sample oscillation frequency and amplitude respectively, m is the magnetic moment of the sample and C is the coupling constant.

2.3.2 Procedure for magnetization measurements:

The samples are mounted on quartz sample holder with the help of a stand, provided with a mirror for centering the sample position. The quartz holder is attached in the sample probe, which is inserted into the sample chamber of the SQUID. In case of high temperature magnetic measurements the sample is fixed to the holder with adhesive named ZIRCAR cement. On completion of the measurement and attainment of room temperature the cement is removed from the pellet by soaking the pellet with alcohol and gently rubbing. There are different standard measurement techniques. One in which sample is magnetized by a constant magnetic field and the change in magnetic moment of the sample with respect to temperature change is measured, producing a DC magnetization curve with temperature. During Field Cooled (FC) measurements, a constant field is applied while cooling and the magnetization data is recorded in presence of that constant field applied before. For Zero Field Cooled (ZFC) measurement, no field is applied while cooling and data is recorded in presence of a constant field. In other method, at a fixed temperature magnetic moment of the sample is recorded with oscillating external magnetic field whereby Moment vs External field graph (M vs H) is obtained. In our case reported here, all the magnetic

susceptibility measurements that have been carried out in various different temperature ranges between 2 K to 390 K as well as in the high temperature range (300-1000 K).

2.4 Dielectric measurement:

The dielectric constant of a material is the measure of the relative permittivity of a material. It can be obtained by capacitance measurement and the corresponding energy dissipation which is known as dielectric loss can be obtained by loss measurement. The charge stored in a capacitor is Q = CV where, C is the capacitance and V is the applied voltage. For a parallel plate capacitor, the capacitance can be written as:

$$C = \varepsilon_0 \varepsilon_r A/d$$

Where ε_0 is the permittivity of vacuum and ε_r is the relative permittivity of the media. In the dielectric study the dielectric constant and loss is measured with respect to temperature or frequency or both. The dependence of dielectric constant and loss on frequency is very important for understanding the dielectric nature of a material. The dielectric loss is indicative of some dielectric relaxation. Dielectric relaxation is the response of non-interacting dipoles to an external ac field. Briefly, when an AC signal is applied, the dipoles try to follow the polarity of the signal but after a certain frequency the dipole cannot follow the polarity and relaxes. In our study, Agilent 4294A Impedance analyzer was used to measure the dielectric constant and loss over the range of frequency 10 kHz to 1 MHz .

2.5 Morphology study (FESEM and TEM):

The surfaces of the compounds as prepared via numerous techniques can be viewed via scanning with high energy beam of electrons. The image is called as Scanning Electron Microscope (SEM) image. In order to acquire image the electron gun at the top of a column

produces high energy electron beam which is passed through vacuum to a selected spot in sample specimen. This beam is scanned in a particular pattern over the specimen whereby secondary electrons are produced on the surface of the specimen and are detected. The secondary signal amplitude varies according to the topography of the specimen. Even if the magnification of SEM can be very high, still in reality it depends on the properties of the specimen, preparative method and other instrumental parameters like accelerating voltage beam intensity etc.

Transmission Electron Microscopy (TEM) uses high energy electron beam to image internal structure through interaction between specimen and electron beam. The small de Broglie wavelength of the electrons results in generation of very high resolution. This leads observer to view very detailed image of the specimen. In TEM, the electron beam is condensed before projecting onto the specimen and after passing through the specimen is magnified.

2.6 Thermogravimetric analysis:

Thermogravimetric analysis is a quantitative technique in which the physical and chemical properties of a material are interpreted by estimation of mass of the material as a function of temperature. It is carried out to characterize thermal stability of a material as well as to detect presence of impurity, crystalline water, adsorbed gases or even presence of mixed valent sites. A TGA consists of a small sample container that is supported by a high precision balance. That container is heated or cooled during the experiment by means of precision heating while the mass of the sample is monitored. During experiment the environment is controlled via purging gas into the system. The gas may be inert or a reactive gas that flows over the sample and exits through an exhaust.

2.7 Optical characterization:

Optical characterization techniques that can be applied for a material are numerous in terms of types and purpose and thus have found a strong ground in modern day research. It includes microscopy, ellipsometry, photoluminescence, absorption spectroscopy, raman spectroscopy, cathodoluminescence etc. During our course of study, we have used UV-Vis spectroscopy and Raman spectroscopic technique and some of the microscopic technique extensively. The microscopic techniques have already been discussed above. UV-Vis technique is basically spectroscopic technique that uses light energy in the ultraviolet to visible region ($\lambda \sim 10^{-9} - 10^{-6}$ m). In this energy spectrum molecules undergo different transitions and thus the method is very commonly used in different type of basic studies. The method is quantitative and can be applied for solid liquid and even for gases also. Our study includes UV-Vis study of both solid and liquid specimen. Liquid phase UV-Vis was carried out in absorption mode while solid phase UV-Vis was carried out in reflectance mode. Thus in solid phase UV-Vis experiment the data in reflectance intensity is converted to absorbance equivalent unit known as Kubelka-Munk unit (K.M unit). Conversion to K.M. unit is based on certain assumptions which are:

I. Particles are randomly distributed,

II. Particle average diameter is less than wavelength of incident light,

III. Incident light diffuse and thus no regular reflections occur.

The expression of Kubelka Munk function is:

$$F(R) = (1 - R)^2 / 2R = k/s$$

Where R is the reflectance of the solid, and k and s are absorption and scattering coefficient respectively.

Raman spectroscopic technique is very much applicable for chemical identification,

molecular structure, bonding characterizations. In this technique light interacts with material (molecule or lattice) and scattered radiation of different wavelengths is produced. Now this scattering has different components like Rayleigh, Stokes or Anti-Stokes scattering. In Raman scattering change in wavelength of scattered light is observed which helps in determining structural and chemical information. Molecules have their rotational, vibrational or electronic energy level transitions in the same energy scale as that of the change in scattered light frequency and thus this technique becomes very fruitful.

In our study, PerkinElmer Lambda 900 spectrometer was used for UV-Vis characterization while Raman spectra were recorded at different spots of the specimen using Jobin Yvon LabRam HR spectrometer.

2.8 XPS study:

X-ray Photoelectron Spectroscopy (XPS), the most widely used surface analysis technique is based on photoelectric effect. The effect is the response of the core shell electrons of an atom by coming out on exposure to external photon beam. For this to happen, the photon energy has to be of higher value than the sum value of electron binding energy (E_B) and the Work Function (φ) between Fermi level (E_f) and Vacuum level (E_v). Thus the resultant kinetic energy of the photoelectrons can be expressed as:

$$E_K = h\upsilon - E_B - \varphi$$

thus,

$$E_B = h\upsilon - E_K - \varphi$$

As each element has its own characteristic core electron levels, thus the XPS peaks will be characteristic of elements. Again the oxidation state of an element largely alters the binding nature and thus the binding energy. The XPS peaks are very much dependent on that and thus the technique has found a solid ground in determining elements and their oxidation states. XPS technique can detect most of the elements except Hydrogen and Helium due to their low

intensities. Since most of the elements have their core levels in the range of 0 – 1000 eV, Al or Mg are used as anode material. The most intense lines ($K_{\alpha 1}$ and $K_{\alpha 2}$) often come as single one and for these two materials they are 1253.6 eV (Al) and 1486.6 eV (Mg). In the instrument a hemispherical analyzer is used to filter the electrons according to kinetic energy criterion. The filtered electrons are further focused by electrostatic repulsion towards specimen.

In the thesis the reported XPS studies have been carried out using Omicron SPHERA analyzer with non-monochromatic X-rays. The deconvolution was carried out in standard software using voight profile fitting.

2.9 Photocatalysis:

Chemically photocatalysis is explained as acceleration of a light induced reaction in the presence of a catalyst. The concept of photo-generated catalysis is based on semiconductor photochemistry and the activity of the catalyst depends on the ability of the catalyst to generate electron-hole pairs which may further lead to generation of different species like free radicals etc. There are two types of photocatalysis viz. Homogeneous and Heterogeneous photocatalysis. Homogeneous type has both the reactants and the catalysts in the same phase while in the heterogeneous type they are in different phases. In present days, heterogeneous photocatalysis is a broad area of research in large number of reactions: mild or total oxidations, dehydrogenation, hydrogen transfer, $^{18}O_2$–$^{16}O_2$ and deuterium-alkane isotopic exchange, metal deposition, water detoxification, gaseous pollutant removal etc. Thus being of very much applicability in different high impact fields the sub disciplines that have been studied here are splitting of water into constituent elemental forms and dye degradation. Photocatalytic water splitting is a terminology used to explain the dissociation of water into its constituent elements with the use of artificial or natural light

source. Production of H_2 fuel has gained increased attention as oil and other non-renewable fuels are becoming increasingly extinct and thus expensive. Hydrogen fuel, which burns cleanly, can be used in a hydrogen fuel cell. Water splitting has grabbed particular interest since it utilizes water, an inexpensive renewable resource. One more positive aspect of this method is it uses powder in solution and sunlight to dissociate water and can thus capable of providing clean, renewable energy. The band gap of the materials has to be greater than 1.23 eV at pH = 0. For the material to be called as potential photocatalyst the ratio of both the gases getting evolved on application of this has to be 2 : 1. Again some materials are seen to be degrading or decaying in terms of activity. For them use of sacrificial agents are recommended. Degradation of organic compounds on the other hand has found importance due to applicability in high impact areas like reduction of environmental pollution and thus reducing environmental degradation. Dyes among them are optically active and thus their degradation can be easily detected via standard regular optical methods.

Here we have tested La_2CrO_6 as a photocatalyst. It was seen to be generating hydrogen from dissociation of water and have degraded very common organic dye Methylene Blue. Visible light radiation source that was used for these two experiments was 400 W Xe lamp, Newport 69920 with flux of ca. 2500 W m^{-2}. In case of water splitting experiment, PerkinElmer Clarus ARNEL 580 gas chromatograph was used to detect gaseous aliquots. In order to evaluate the dye degradation, UV-Vis spectroscopic technique was considered and for this, PerkinElmer Lambda900 spectrometer has been taken help of.

2.10 Bibliography:

1. Rietveld, M., H.; Acta Crystallographica. **1967**, 22, 15.
2. Rietveld, M., H.; Journal of Applied Crystallography.**1969**, 2, 65.
3. Pecharsky, K.; Vitalij, Zavalij.; Y, Peter; US Springer. **1974**, 777, 133.

4. The measurement, instrumentation, and sensors handbook. 32-113, 1999.

Chapter 3

Synthesis, characterization & photocatalytic activity of La_2CrO_6 with unusual chromium (VI) oxidation state

3.1

Introduction:

Partial or complete filling of *d* electrons make the transition metals to possess several different oxidation states. These different oxidation states of transition metal ions in oxides are very important and known to affect the magnetic, electrical and optical properties of various compounds. Transition metal oxides with transition metal ion in its highest possible oxidation state are especially of significant importance because of their superior dielectric properties. For example $BaTiO_3$, $BaTaO_2N$ *etc*. are high dielectric materials with former being well known also for its room temperature ferroelectric properties [1-3]. d^0 electronic configuration is considered to be a prerequisite for exhibiting spontaneous polarization in classical ferroelectric compounds. Recently, one more aspect of this d^0 ness has been exploited which is the oxidation and/or reduction of water in the presence of light using such materials as catalysts. The absence of electrons in the conduction band has been shown to enhance the activity towards water oxidation and/or reduction. The valence band for d^0 systems is composed of O 2*p* orbital while the conduction band is constructed by *d* or *sp* orbital [4]. The positions of these bands as compared to the redox potentials of H_2 and O_2 decide the catalytic activity. Materials like TiO_2, WO_3, Ta_3N_5, $SrTiO_3$ *etc*. have been shown

to oxidise and/or reduce water depending on their position of valence band maxima and conduction band minima relative to the oxidation and reduction potential of water [4].

Rare earth chromium oxides, RCrO$_3$ and RCrO$_4$ (R = rare earth) have been extensively studied. RCrO$_3$ are orthorhombic perovskites with canted antiferromagnetic ordering of Cr (III) ions [5]. Recently, some of them have also been shown to exhibit multiferroic properties [5]. Among RCrO$_4$, LaCrO$_4$ has monazite type monoclinic structure whereas other members of the group (R = Nd - Lu) are zircon-type with tetragonal structure [6-7]. Most of the members show antiferromagnetism with T_N less than 30 K. Highest possible oxidation state of chromium with d^0 electronic configuration is VI and is commonly found in salts like K_2CrO_4, $K_2Cr_2O_7$ and $SrCrO_4$. Other Cr (VI) compounds have rarely been investigated in the literature. A common impurity of La_2CrO_6 containing Cr (VI) is often observed in the solid solutions of La_2O_3 and Cr_2O_3 [8]. Properties of this compound in the pure bulk form are not yet studied to the best of our knowledge. Recently, thin film of La_2CrO_6 were prepared and characterized [9]. Highly crystalline powder of La_2CrO_6 was also prepared by exchange reaction of LaOCl and K_2CrO_4 but the properties were not studied [10]. Herein, we report the synthesis of La_2CrO_6 nanoparticles by citrate based sol-gel method along with their optical, magnetic and photocatalytic activity.

3.2
Scope of investigation:

Ever decreasing fossil fuel storage as well as ever increasing harmful effects in using these has become a major concern and as a result, for the past few decades people are trying to switch over to clean and renewable energy source. Even if solar energy (power level 1000W / m^2) [11-12] is more than sufficient for earth energy needs, the electrochemical [13-14] and photovoltaic cells [14] are costly to fabricate and not much efficient. Thus if one

considers a concrete solution, H_2 seems to be promising source of clean energy and in parallel water can be the most easily available environment friendly source of hydrogen. On this important economic and environmental interest, people are trying to design materials that can show photocatalytic activity in splitting water into constituent H_2 and/or O_2. Lots of different compounds having d^0 electronic configuration that can catalytically split water to generate H_2 and/or O_2 have been synthesized so far [4]. The photocatalytic property of heterogeneous oxide semiconductors in splitting water initiates via absorption of photon resulting in separation of electron and hole in the band gap of the material [4]. Depending on the band gap and position of valence and conduction band the separated protons and electrons move and react with water. La_2CrO_6 being a d^0 compound holds strong probability of having catalytic properties. The yellow colour of the as prepared compound also indicated that the compound must absorb violet colour according to Newton's colour wheel the energy window of which has a fair chance of matching or even exceeding water dissociation energy criteria. Thus prepared by a new method, characterization was carried out of all the basic properties like optical, magnetic electrical etc. and based on these applicability of this compound was also checked.

3.3.

Experimental Section:

3.3.1 Chemicals:

Lanthanum oxide (La_2O_3) was purchased from Sigma Aldrich chemicals. Chromium nitrate nonahydrate [$Cr(NO_3)_3$. $9H_2O$] was purchased from Sigma Aldrich chemicals. Citric acid ($C_6H_8O_7$) was purchased from SDFCL. All the reagents were AR grade. Lanthanum oxide was preheated at 900°C in air for 12 hours in order to remove the adsorbed CO and

moisture. Deionized water with resistivity in the range of MΩ was obtained from Millipore ultrapure water purification system.

3.3.2 Synthesis:

In 50 mL of deionized water, 0.7330 gm (2.249 mmol) of La_2O_3 was added and was dissolved via drop wise addition of conc. HNO_3 into the solution. Under constant stirring, 1.8002 gm (4.499 mmol) of $Cr(NO_3)_3.9H_2O$ was added into the solution followed by addition of 3.455 gm (17.998 mmol) of Citric Acid. Thus the citric acid concentration was exactly the double of total cation concentration. The whole solution was kept exposed to air under continuous stirring at 98 °C such that solvent water evaporates slowly as well as the citrate complex gel precursor gets formed. This resultant gel precursor was then heated and dried for overnight at 200 °C. The product obtained was heated at 600°C at a rate of 5 °C /min in oxygen flow for 5.5 hours in order to drive off the amorphous carbon in the form of CO_2. For comparison, this final calcination temperature was varied from 550 °C to 800 °C and compounds collected at two different temperatures 600 °C and 800 °C named S_1 and S_2 respectively were considered for further investigations selectively.

3.3.3 Photocatalytic methods:

For dye degradation studies, 4 mg of the compound was added to 20 mL of aqueous solution of 15 μM methelyne blue (MB) in a cylindrical quartz vessel. The mixture was sonicated for 15 min followed by stirring for 30 min in dark. 1 mL of the mixture was then taken, centrifuged and the absorption spectra of the supernatant was recorded. This is known as dark reading. The vessel was then irradiated with visible light by exposing it to 400 W Xe lamp (Newport) fitted with a 12 cm path length of water filter to cut off IR radiation and a 400 nm cutoff-filter. One mL of the mixture was taken out at an interval of 20 min for 2 h for

recording UV-vis spectra. Time interval was increased at latter part of the experiment. The compound dispersed in the mixture was centrifuged out before UV-vis experiments to avoid scattering. Photocatalytic H_2 evolution experiments were carried out in quartz fitted with a septum for removal of the gaseous product from the head-space. 400 W Xe lamp was used as the light source with 12 cm water filter for removal of IR radiation and 400 nm cut-off-filter to block the UV-light. Photocatalytic reduction of water was carried out by dispersing about 5 mg of the sample in a solution of 0.1M Na_2SO_4 and 0.1M Na_2S. Two milligrams of the compound was dispersed in 50 mL of water by ultrasonication and the vessel was later purged with N_2 to remove all gases before irradiation. The evolved gases were analysed by gas chromatography using a Perkin-Elmer Clarus 580 GC with 500 μL gas collecting loop. 1 mL of the evolved gases was injected manually every 1 h for analysis.

3.3.4 Characterization:

The products were characterized by X-ray diffraction technique using Bruker Discover D8 advance diffractometer with Cu *Kα* radiation, (λ=1.54 Å, step size: 0.02, current: 30 mA and voltage: 40 kV). Field-emission scanning electron microscopy (FESEM) images and energy-dispersive analysis of X-rays (EDAX) were obtained by use of FEI (Nova-Nano SEM-600 Netherlands) instrument. TEM measurements were performed on a JEOL, JEM 3010 operated at 300 kV. Samples were prepared by placing a drop of dispersion on a TEM grid (holey carbon). Raman spectra were recorded at different locations of the sample using Jobin Yvon LabRam HR spectrometer with Ar laser. Diffused reflectance and absorbance data in UV-Vis range were collected in Perkin-Elmer Lambda 900 spectrometer. 1 mm path length cuvette was used for recording the spectra. Thermo gravimetric analysis was done using Pyris 1 TGA. Magnetic measurement was done using vibrating sample magnetometer squid by Quantum design. FC and ZFC measurement were carried out at

external dc field of 1000 Oe from 2 K to 300 K whereas M vs. H measurement was carried out at 300 K. For photocatalysis experiments visible light radiation source that was used was 400 W Xe lamp, Newport 69920 with flux of ca. 2500 W m^{-2}. In case of water splitting experiment, PerkinElmer Clarus ARNEL 580 gas chromatograph was used to detect gaseous aliquots. In order to evaluate the dye degradation, cuvette of 1 mm path length was used. UV-Vis data of the dye solution were recorded with the help of PerkinElmer Lambda 900 spectrometer.

3.4.

Results and discussion:

3.4.1 Synthesis:

Polycrystalline La_2CrO_6 has been prepared via exchange reaction between rare earth oxychloride (LaOCl) and alkali chromate (best with K_2CrO_4) [10]. Solid state synthesis of the compound is also reported where stoichiometric mixture of La_2O_3 and Cr_2O_3 has been pelletized and heated under oxygen flow [15]. Recently thin film of La_2CrO_6 has been prepared [9]. Co-precipitation method using $La(NO_3)_3.6H_2O$ and $Cr(NO_3)_3.9H_2O$ has resulted in formation of mixed phases [8]. Here the compound has been synthesized via citrate sol gel technique (c.f. fig. 3.1.). La_2O_3 was dissolved in water with addition of nitric acid drop wise which hydrolysed the oxide into La^{3+} and NO_3^-. Citric acid was used in

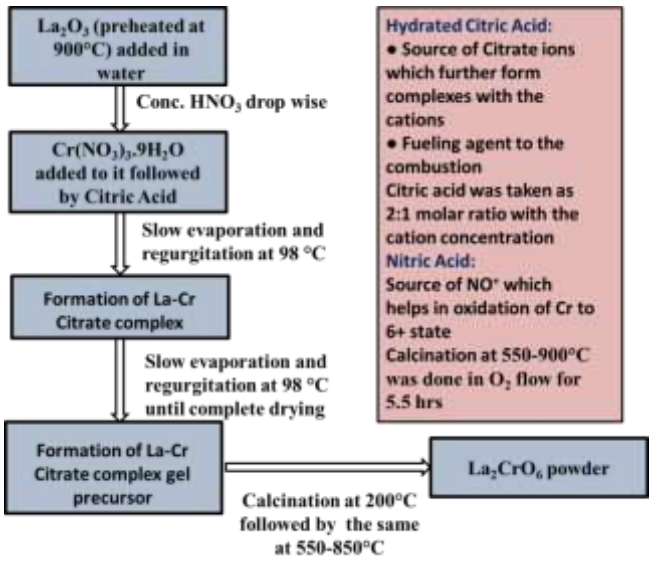

Figure 3.1. Illustration of sol-gel method

2:1 stoichiometric molar ratio with respect to cation concentration. It acted as complexing agent as well as fuel. It has flash point at around 200 °C and thus oven temperature was maintained at the same.

3.4.2 Crystal Structure:

Compound was found to be crystallizing in monoclinic structure with *C*2/*c* space group. S_2 was much more crystalline than S_1 due to heating at higher temperature and thus was more appropriate for structural refinement. XRD θ-θ scan data of S_1 and S_2 have been shown in figure 3.2. (a). For S_2 Rietveld refinement along with the structure shown in figure 3.2. [(b) & (c)] confirms of the crystallization of the compound in single phase monoclinic

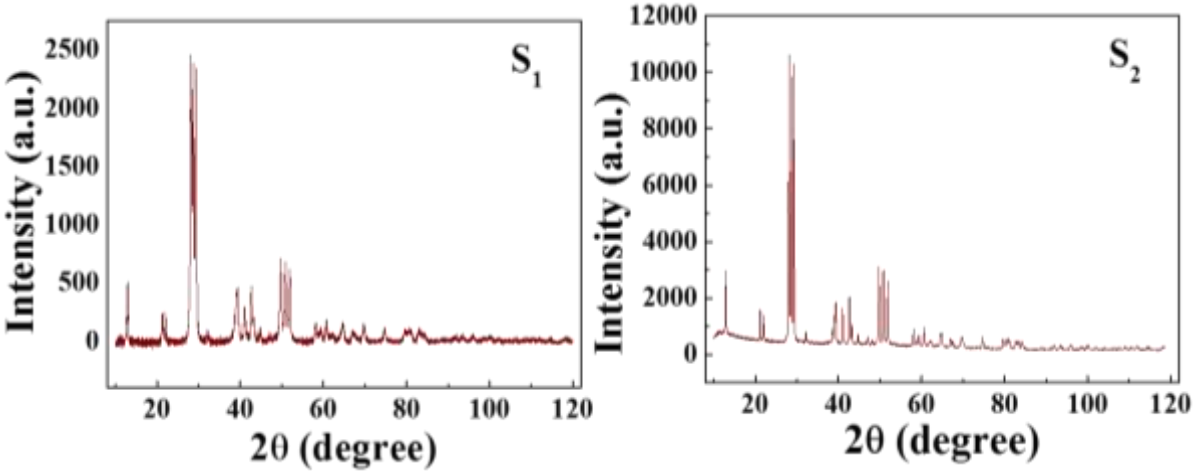

Figure 3.2. (a) XRD patterns of S_1 and S_2 heated for same duration. Intensity comparison tells that the S_2 crystal quality is far superior to S_1.

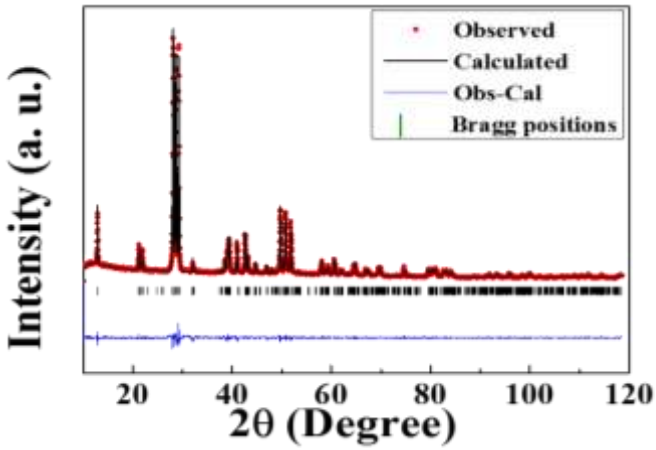

Figure 3.2. (b) Reitveld refinement plot of La_2CrO_6

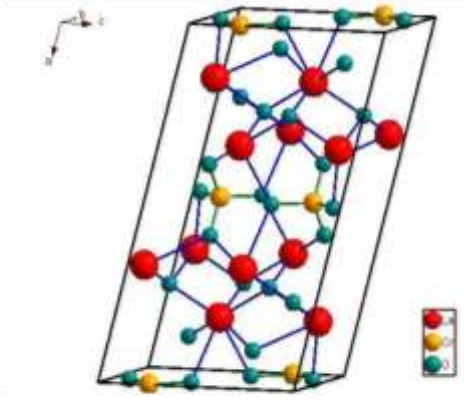

Figure 3.2. (c) Monoclinic structure of La_2CrO_6.

structure. The layered compound is consisted of the extended $[La_2O_2]^{2+}$ layers with tetrahedral $[CrO_4]^{2-}$ accommodated in between. The cell parameters are a = 14.3194 (5) Å, b = 4.4013 (1) Å, c = 8.4818 (3) Å. They have shown that because of strain generated in excessive stretching of $[La_2O_2]^{2+}$ layers the rigid tetrahedral $[CrO_4]^{2-}$ ions get accommodated but the oxygen atoms show different types of bonding with the metals.

3.4.3 Morphology:

The porosity of the material typical of a sol-gel product was confirmed from FESEM {c.f. figure 3.3. (a) and (b)}. Particles with pore diameter in the range of 8-30 nm were formed in case of S_1. For S_2, pore diameter was one or two order higher. Grain size in the range of 250 nm -2 μm and 3-12 μm was seen for S_1 and S_2 respectively. HRTEM image of good clarity showing lattice fringes could not be obtained as the surface of the particles were changing with time. Surface charging or breakage of lattice grids on exposure to e^- beam can be accounted for this. The SAED ring pattern shows polycrystalline nature of the sample.

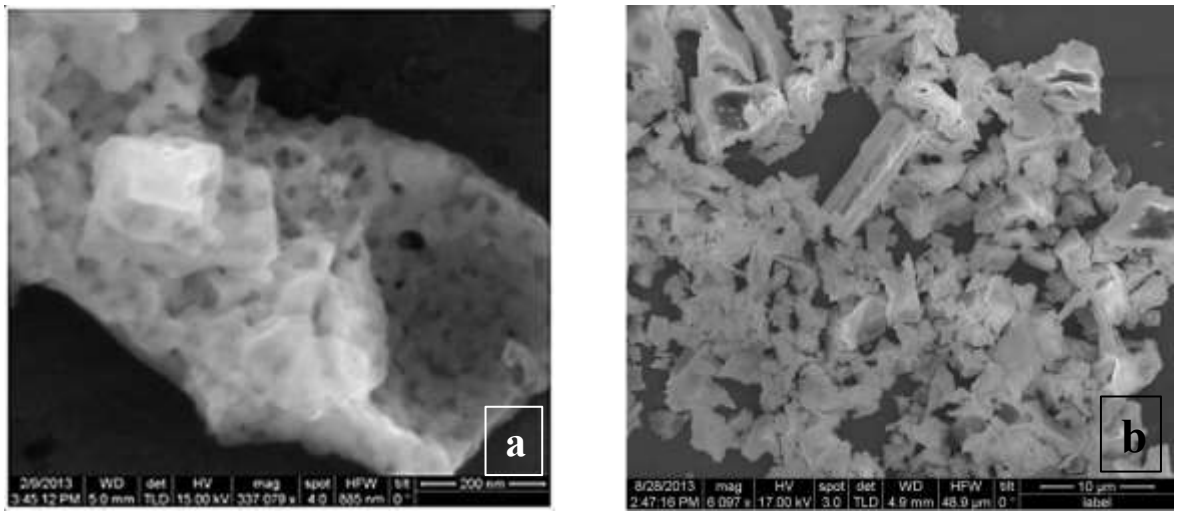

Figure 3.3. (a) FESEM image of S_1 showing aggregation in the range of 250 nm- 2 μm.**(b)** FESEM image of S_2 showing agglomeration in the range of 3-12 μm.

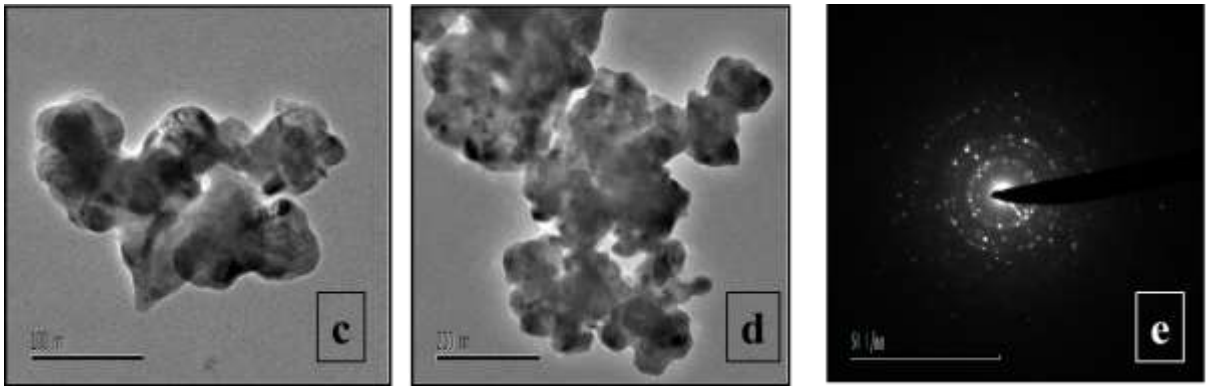

Figure 3.3. (c) & (d): TEM image of agglomerated particles. **(e):** SAED pattern showing polycrystalline nature owing to agglomeration.

3.4.4 Thermogravimetric analysis:

Thermogravimetric analysis was done both in oxygen and nitrogen atmosphere at 5 K min^{-1} rate. Interestingly much difference was seen between the two results. In oxygen atmosphere increase in weight percentage was observed at different regions of temperature. Increment of 0.8 weight percentage was seen in the temperature range of 280-890 °C. This cumulative increase is very uncommon and the exact reason is unknown. Possibly the reason might be the presence of impurity phases of lower oxidation states which can take up O_2 and get oxidised at higher temperature. At 897 °C sharp fall in weight percentage was seen which is indicative of decomposition of the compound. XRD of the residue left shows presence of $LaCrO_3$, $LaCrO_4$, La_2O_3 phases thus supporting the fact of decomposition. Although the

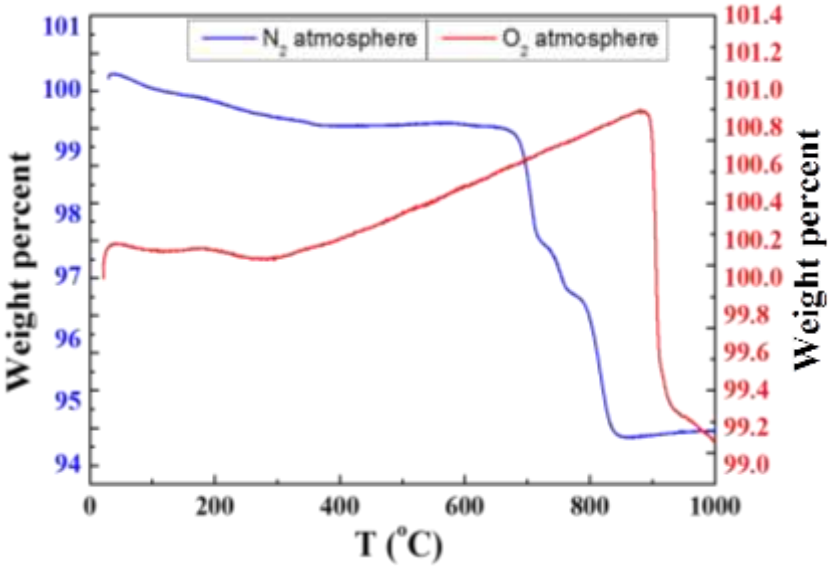

Figure 3.4. TGA graph of La_2CrO_6 in different atmosphere. The red curve shows the change in weight percentage while heating in O_2 atmosphere while the blue one depicts the same in N_2 atmosphere.

direct proof like favourable energy condition or anything else that is supportive of this analogy is not known, still the nature of the compound on N_2 atmosphere (figure 3.4. blue curve) is supportive of this. In N_2 atmosphere the compound was getting decomposed at much lower temperature (at 670 °C) and the decomposition was stepwise not like that in case of O_2 atmosphere. $LaCrO_3$ and $LaCrO_4$ were confirmed as residue after decomposition via XRD technique.

3.4.5 Magnetic properties:

Figure 3.5. {(a) and (b)} shows the Field Cooled (FC) at 1000 Oe and M vs. H at 300 K characteristics respectively. S_2 was selected for the measurements as it was having more crystallinity. For the d^0 electronic configuration of the compound magnetic property has to be of diamagnetic type. Thus the field cooled (FC) plot had to be linear with zero slope at negative magnetization. Instead, considerable amount of paramagnetic nature has been seen which further decreases with increase in temperature as well as with sintering. Thus this anomaly can be attributed to different defects present as due to sintering thermal diffusion increases, and as a result of this, the concentration the defects decreases.

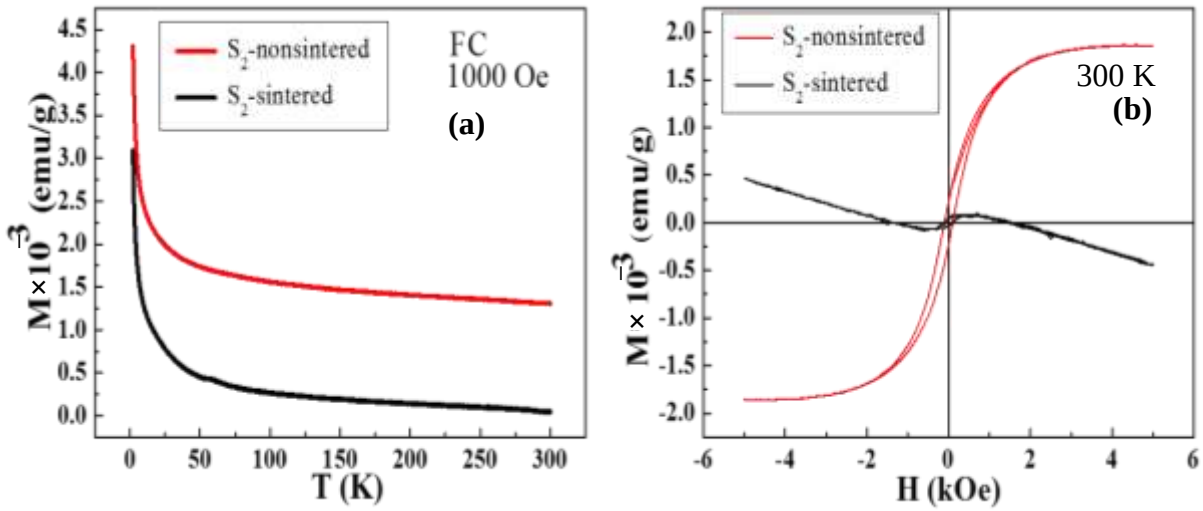

Figure 3.5. (a) FC data (1000 Oe). The red curve is for non-sintered S_2 while black one is of the sintered S_2. **(b)** M vs. H comparative plot of non-sintered and the sintered S_2.

M vs. H curve shows defect contributed ferromagnetic behaviour with very low value of retentivity and coercivity. We say it is originated from defects mostly in the form of lattice disorder because the saturation magnetization decreases with sintering as the defect concentration decreases with it.

3.4.6 XPS study:

XPS study was carried out on both S_1 and S_2 whereby evidences on multiple oxidation states along with presence of defects were found. The VB spectra for S_1 was not conclusive, thus S_2 VB spectra has been shown here {c.f. figure 3.6. (a)}. Valence band position was found to be at + 0.40 eV. Strikingly even after Fermi energy level considerable amount of intensity was observed which means above Fermi level multiple numbers of associated electronic states are present. This can happen in two cases, one when the material is conducting and the second, when defect states are present there in between valence and conduction band. Herein the second case can be accepted as we have found our compound to be semiconducting in nature via optical and electrical measurements explained later. Both S_1 and S_2 data had deviation of around 4-5 eV (C 1*s* peak) which means charging was occurring in both samples. Defect states are potential sites where in general charge neutrality condition is not maintained and thus on exposure to external bias these sites can get charged up very easily. Thus they can be probable reason behind this incident. Moreover, the

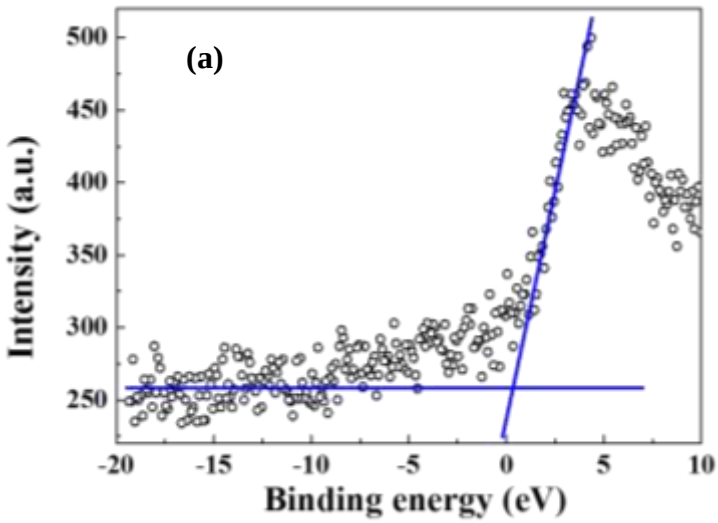

Figure 3.6. (a) Valence band spectra of La_2CrO_6

low thermal stability of La_2CrO_6 does not lead to complete and efficient thermal diffusion. This is very much supportive condition for defect formation.

De-convoluted Cr $2p_{3/2}$ core level spectra for samples S_1 and S_2 {c.f. figure 3.6. (b) and (c)} show presence of oxidation states other than the expected Cr (VI). In figure 3.6. (b), the principle peak at binding energy 579.79 eV corresponds to Cr (VI) oxidation state [16]

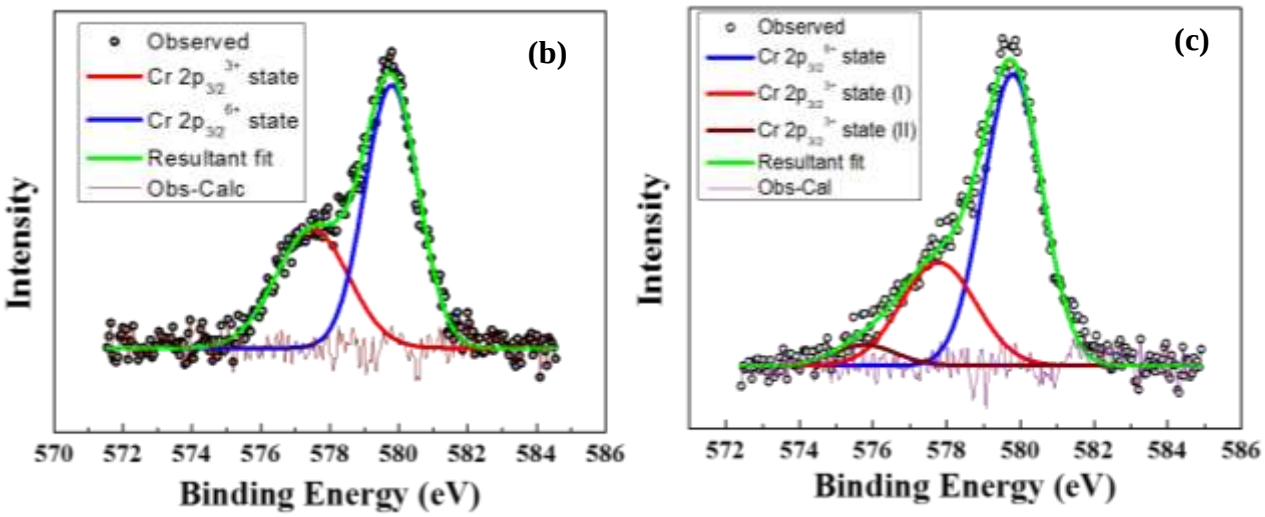

Figure 3.6. (b) & (c) De-convoluted Cr $2p_{3/2}$ core level XPS spectra of S_1 and S_2 respectively.

while the peak at 577.44 eV can be assigned to Cr (III) [17].Similar nature is seen for S_2 as seen in figure 3.6. (c). Peak at 579.7 eV represents presence of Cr (VI) state [16] while lower binding energy peaks at 577.7 eV and 575.6 eV are representative of lower oxidation states ($3 < n < 5$) most probably of Cr (III) [17-18]. The reason behind the difference between two Cr (III) binding energy positions is due to the different environment around them. The association with Cr (VI) play role in the binding energy position also. Thus from XPS data it can be ascertained that the compound was containing defects as well as multiple oxidation states. Being a surface characterization technique XPS cannot tell about the bulk and thus these abnormalities are present at the surface only. Long-time X-ray diffraction scan of both the samples could not find any impurity even to smallest extent. Thus presence of these

different oxidation states at the bulk is ruled out. They are possibly of negligible amount and are localized at the surface.

3.4.7 Optical properties:

3.4.7.1 UV-Vis and PL study:

As determined via diffused reflectance spectroscopy, the compound bright yellow in color was found to be absorbing at around 396 nm as exposed to UV-Vis spectra {c.f. figure 3.7.1. (a)}. Thus according to Newton's color wheel the yellow La_2CrO_6 absorbs violet color and yellow color becomes visible.

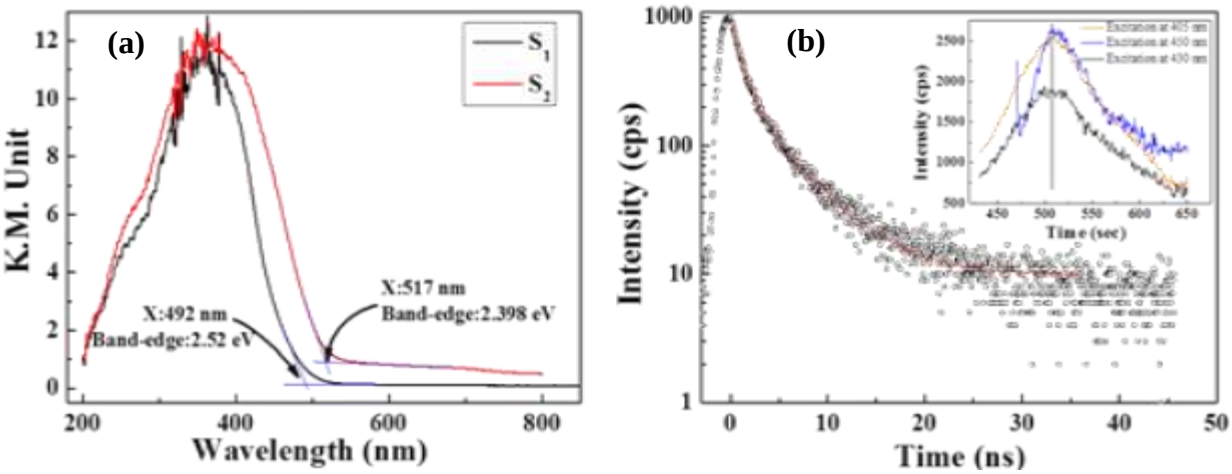

Figure 3.7.1. (a) UV absorption spectra of S_1 and S_2 carried out in diffused reflectance mode. The red graph is representative of S_2 while black one is of S_1. **(b)** Lifetime study of S_2. Inset shows steady state measurement at different excitations.

The optical band gap of S_1 was found to be 2.52 eV while that of S_2 was 2.39 eV. Having noble gas electronic configuration at 6+ oxidation state, it is impossible for Cr to show colour due to *d-d* optical transition. The absorption thus occurs due to transition between 2*p* orbital of oxygen and 3*d* orbital of Cr. Experimental study supported by DFT calculation performed by Qiao *et al.* supports the same [8]. The photoluminescence study was carried out keeping

the defect states in mind. Steady state measurement was carried out by exciting at 405 nm, 430 nm and 450 nm. Data at different excitations has been shown in figure 3.7.1. (b) Inset. The excitation peak does not vary its position with the change in excitation energy which implies that the transition characteristics are inherent of sample not of defects. Lifetime study {c.f. figure 3.7.1. (b)} was carried out for excitation at 405 nm. Decay nature was found to be of double exponential type, defect lifetime being ~1 ns while that of compound is 4.6 ns.

3.4.7.2 Raman Study:

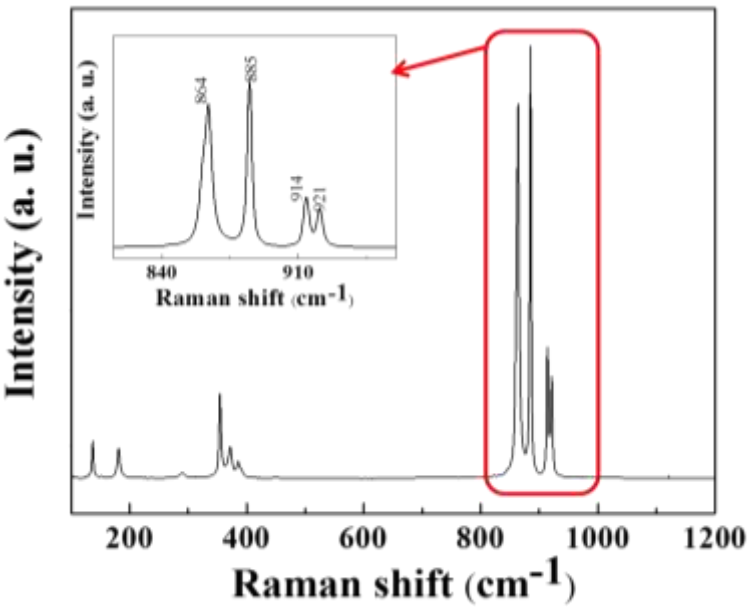

Figure 3.7.2. Raman spectra showing presence of single phase La_2CrO_6 with no additional phases of possible impurities.

Thus, until now it is seen that the compound contains defect states as well as mixed oxidation states at the surface. In an effort to investigate the possibility of presence of compounds consisting of chromium in different molecular states, Raman spectroscopic study was performed. Identification was based on comparison with the data available. Shown in figure 3.7.2., the RS data surprisingly does not show a single peak corresponding to oxide of La and Cr or lower valence chromate. RS peaks at 139 cm^{-1}, 181 cm^{-1}, 355 cm^{-1}, 371 cm^{-1}, 384 cm^{-1} (having low intensities) and 865 cm^{-1}, 885 cm^{-1}, 914 cm^{-1} and 921 cm^{-1} corresponding to La_2CrO_6 have been seen [19]. Possibility of formation of La_2O_3, Cr_2O_3 $LaCrO_4$ and $LaCrO_3$ can thus be ignored.

3.4.8 Electrical properties:

The nature of the dependence of resistivity (in log scale) on temperature as well as the value of resistivity infers that the compound is semiconducting in nature. Resistivity fall in the order of 8 was seen and it was seen to be almost stable at around 330 K. Thus it can be said that abnormal intensity above Fermi level in XPS VB spectra {c.f. figure 3.6. (a)} is due to defect states being present in between valence and conduction band. The

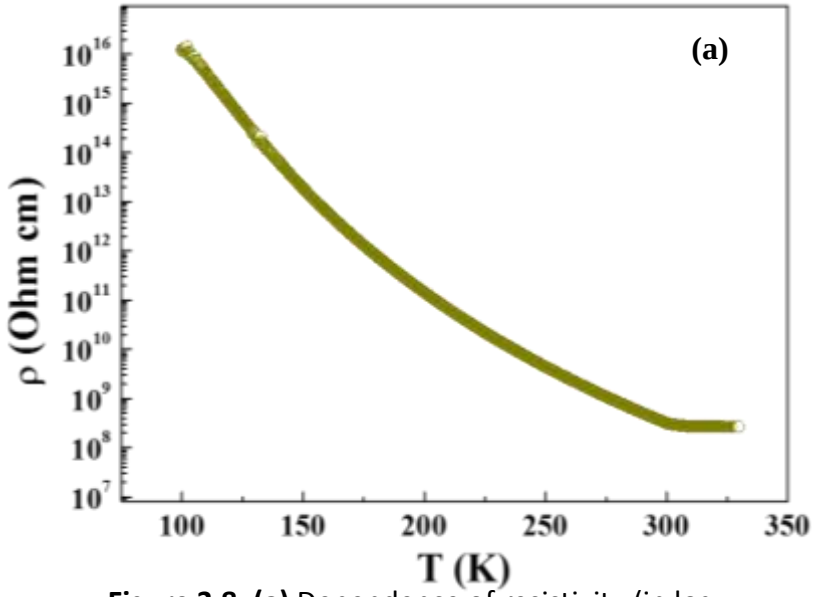

Figure 3.8. (a) Dependence of resistivity (in log scale) on temperature as measured in an external positive bias of 50.4 V.

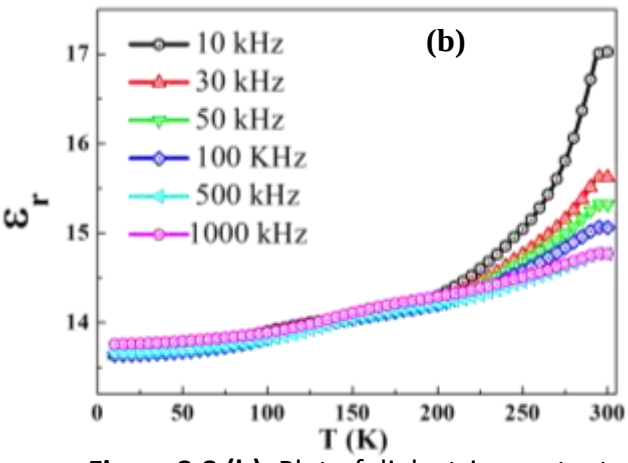

Figure 3.8 (b). Plot of dielectric constant in the temperature range of 10-300 K.

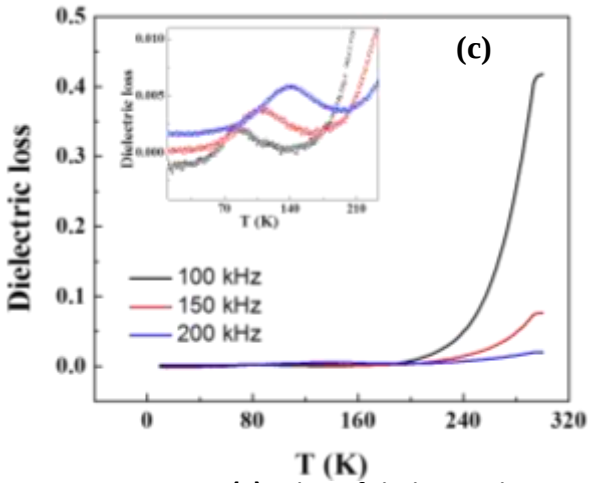

Figure 3.8 (c). Plot of dielectric loss in the temperature range of 10-300 K. Inset shows temperature dependence of the anomaly.

dielectric constant of the material was seen to be decreasing with temperature as can be seen from the figure 3.8. (b). The increase in ε_r is consistent with increasing temperature. As the dc conductance increases it increases the permittivity of the material. Accordingly the dielectric

constant becomes higher. Again as the dielectric constant increases with T the dielectric loss should be of low value. Instead it is seen to be increasing after 170 °C. Although the exact reason behind this loss is unknown, but reason behind the loss in the form of heat might be the presence of defects which at lower temperature might form local resistive sites and at higher temperature allow current to pass more easily. Thus at higher T resistance (R) decreases and dielectric loss in the form of heat increases (~V^2/R).

3.4.9 Photocatalytic properties:

We have studied the catalytic activity of our sample for the photodegradation of methylene blue (MB) under visible light irradiation. Figure 3.9. shows the time-dependent changes in the absorbance of MB under visible light irradiation. While MB degrades only by only 40% under visible light after five hours it degrades to almost 90% in presence of La_2CrO_6. Greater degradation of MB in presence of La_2CrO_6 is attributed to strong absorption of visible light by the catalyst followed by photogeneration of electrons and holes. The degradation of MB can occur by two processes:

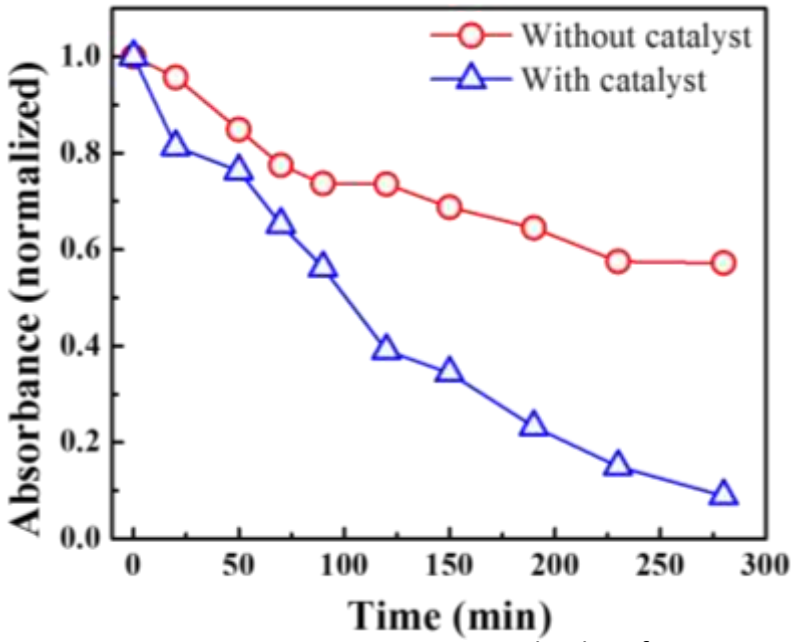

Figure 3.9. Comparative timescale plot of MB (Methylene Blue) degradation.

(i) direct oxidation of MB by the photogenerated hole (h^+)

(ii) generation of OH° through a series of steps involving the photogenerated e^- and the h^+ [20] which then oxidizes MB.

While at higher concentration of MB degradation happens by direct oxidation of MB by h^+, at lower concentrations second process is more probable. The rate constants (k) of degradation of MB in the presence of La_2CrO_6 were calculated using the Langmuir–Hinshelwood rate equation

$$\ln \frac{C_0}{C_t} = kt,$$

where C_0 and C_t are the absorbance of MB at λ_{max} absorption of MB (*i.e* 664.5 nm) recorded at time 0 min and t min. k, the apparent rate constant was found to be 8.6355×10^{-3} min^{-1}.

Photocatalytic H_2 evolution experiments were carried out in presence of Na_2S and Na_2SO_3 as sacrificial electron donors. While control (solution of Na_2S and Na_2SO_3) shows no hydrogen evolution under visible light, in presence of La_2CrO_6 around 100 μmoles of H_2 are evolved per gram of the catalyst with a turn over frequency of ~9 hr^{-1}, turn over frequency being calculated using the formula,

$$TOF = \frac{moles\ of\ Hydrogen\ evolved}{moles\ of\ the\ catalyted\ used\ \times\ time}$$

3.5

Conclusion:

The compound, as prepared by Sol-Gel technique crystallizes in monoclinic centrosymmetric structure (space group *C*2/c) and has bright yellow colour with optical band gap of 2.46 eV (504 nm) as obtained from UV-Vis spectroscopy. Owing to d^0 configuration of Cr (VI), the material should be essentially diamagnetic. However, ZFC-FC and M vs. H

measurements of the powder samples reveal the presence of paramagnetic nature that decreases with increase in particle size due to sintering. The presence of magnetism in small particles is consistent with the presence of multiple oxidation states of Cr at the surface as confirmed by XPS. Interestingly, Raman study confirmed absence of probable lower valence compounds of chromium. This implies that the magnetism of the mainly is defect induced while there might be different oxidation states which are much more localized in nature. In terms of application, supported over XPS and UV-Vis spectroscopy, the material exhibits catalytic activity in photo-degradation of Methylene Blue and evolution of H_2 via water splitting on exposure to visible light.

3.6

Bibliography:

1. Herbert, J. M.; Ceramic Dielectrics and Capacitors, (Gordon and Breach, Philadelphia, 1985).
2. Hewat, A. W.; Ferroelectrics **1974**, 6, 215.
3. Kim, Young-Il; Si, Weidong; Woodward, Patrick M.; Sutter, Eli; Park, Sangmoon; Vog, Thomas; Chem. Mater. **2007**, 19, 618-623.
4. Kudo, A.; Miseki, Yugo; Chem. Soc. Rev. **2009**, 38, 253.
5. Sahu, Jyoti, Ranjan *et al.*, J. Mater. Chem. **2007**, 17, 42.
6. Carter, J. D.; Anderson, H. U.; Shumsky, M. G.; J. Mater. Sc. **1996**, 31, 551-557.
7. Jimenez, E.; Isasi, J.; Saez-Puche, R.; Journal of Alloys Compd. **2000**, 312, 53-59.
8. Kaddouri, A.; Ifrah, S.; Bergeret, G.; Catal. Lett. **2009**, 129, 336–343.
9. Qiao, L. *et al.;* J. Mater. Chem. C **2013**, 1, 4527.

10. Charkin, D. O.; Grischenko, R. O.; Sadybekov, A. A.; Goff, R. J.; Lightfoot, P.; Inorganic Chemistry, **2008**, 47, 3065-3071.
11. Lewis, N. S.; Crabtree, G.; Nozik, A. J.; Wasielewski, M. R.; Alivisatos, A. P. Basic Research Needs for Solar Energy Utilization ; U.S. Department of Energy: Washington, DC, **2005**.
12. Huynh, W. U.; Dittmer, J. J.; Alivisatos, A. P.; Science **2002**, 295 (5564), 2425–2427.
13. Bach, U.; Lupo, D.; Comte, P.; Moser, J. E.; Weissortel, F.; Salbeck, J.; Spreitzer, H.; Gratzel, M., Nature **1998**, 395 (6702), 583–585.
14. Gratzel, M.; Nature **2001**, 414 (6861), 338–344.
15. Kallarackel, T. J.; Gupta, Sapna; Singh, Prabhakar; J. Am. Ceram. Soc. **2013**, 96, 3933–3938.
16. Capece, F. M.; Dicastro, V.; Furlani, C.; Mattogno, G.; Fragale, C.; Gargano, M.; Rossi, M.; J. Electron Spectrosc. Relat. Phenom. **1982**, 27, 119.
17. Wei, J.; Xue, Q.; Wear **1994**, 176, 213.
18. Howng, W. Y.; Thorn R. J.; J. Chem. Phys. Solids **1980**, 41, 75.
19. Hoang, D. L.; Dittmar, A.; Schneider, M.; Trunschke, A.; Lieske, H.; Brzezinka, K. – W.; Witke, K.; Thermochimica Acta **2003**, 400, 153–163.
20. Houas Ammar *et al.* Applied Catalysis B: Environmental **2001**, 31, 145–157.

Chapter 4

Does oxygen deficiency have an effect on spin state transition in $YCoO_3$?

4.1

Introduction:

Among all 3*d* transition metals oxides the cobalt oxides share lot of limelight due to unique character of spin states of cobalt. Like other transition metals, cobalt exhibits several possible oxidation states like Co^{2+}, Co^{3+} and Co^{4+} and several types of coordination, i.e. tetrahedral, pyramidal, and octahedral. As a result, cobalt oxides offer a wide range of field for the creation of both stoichiometric oxides and nonstoichiometric oxides, involving mixed valence of cobalt and/or the presence of oxygen vacancies. The hallmark of cobalt oxides which separates itself from other 3*d* metal oxides is the ability of cobalt to be present in various spin states, that is, low spin (LS), high spin (HS), and intermediate spin (IS) state. The theory behind having these different spin states is very much complicated and has not been completely understood so far. The reason behind this complexity is the fact that the crystal field splitting Δ_{cf} of the 3*d* energy level of the cobalt ion in cobalt oxides is of the same order of magnitude as the Hund's rule intra-atomic exchange energy J_H and the 3*d*-orbital bandwidth which makes these different spin states very much possibility and abundant. Considering octahedral geometry the cobalt oxides have Co^{2+} always in high-spin state $t_{2g}^5e_g^2$ (S=3/2) as decided by Hund's rule while crystal field comes into effect in case of Co^{4+} which takes low-spin state $t_{2g}^5e_g^0$ (S=0). The Co^{3+} instead does not fall among the two mentioned above and shows low-spin $t_{2g}^6e_g^0$ (S=0), high-spin $t_{2g}^4e_g^2$ (S=2) and Intermediate-

spin state $t_{2g}^5 e_g^1$ (S=1). The reason being the ligand effect of O on Co atom and thus the Co-O bond length and Co-O-Co bond angle determine the spin state. Now this geometry depends on external parameters like temperature or pressure. Thus, variation of these parameters or application of applied magnetic field can provoke the spin state transition very easily. Thus depending on the oxidation state, Co shows different properties like high dielectric constant (Co^{2+} and Co^{3+} mixed systems) or magnetic insulation (Co^{2+}) or good thermoelectric properties (Co^{3+} and Co^{4+} mixed systems) [1].

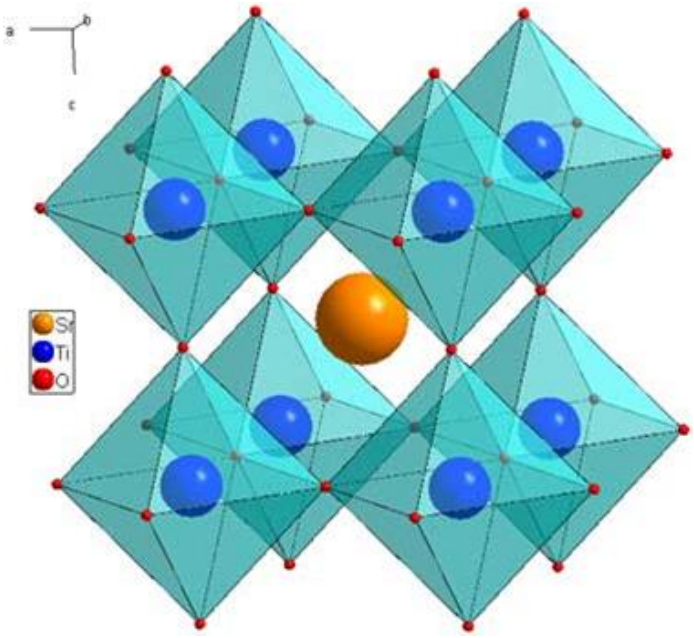

Figure 4.1.: Regular Cubic structure of $SrTiO_3$

The extensive investigations on rare earth cobaltites $LnCoO_3$ (Ln=Y or lanthanides) have been started from long back due to their characteristic structural features and unique magnetic and electronic transition which are related to changes in local spin states of Co^{3+} and the character of itinerant carriers [2-10]. In terms of crystal structure, the stoichiometric cobaltites do not fall under regular cubic perovskite structure characterized by $Pm\bar{3}m$ space group. $LaCoO_3$ crystallizes in rhombohedrally distorted cubic perovskite structure ($R\bar{3}c$) while other cobaltites of the series Ln = Pr to Lu and Y show an orthorhombic distortion of the perovskite cell characterized by the space group *Pbnm* (or the equivalent group *Pnma*).

The size of Ln^{3+} ions governs the magnitude of distortion. The decrease in Ln^{3+} cation radius results the transition of the perovskite structure from higher to lower symmetry. For example, $NdCoO_3$ shows a very small distortion and crystallizes in an almost cubic structure [10]. In all cobaltites, the cobalt ion is found to be surrounded by weakly distorted oxygen CoO_6 octahedra, whereas the rare-earth ions are in distorted cubo-octahedra formed of 12 oxygen ions (Figure 4.1.). Of the 12 Ln-O bonds, 3 are long, 6 are medium-length, and 3 are short bonds. This distortion effectively inverts b > a to a > b and in this fashion structural transition from orthorhombic to rhombohedral symmetry happens [11]. The magnitude of structural distortions changes significantly with the change in temperature also.

In terms of magnetic and electrical properties, the $LnCoO_3$ are seen to be having diamagnetic ground state characteristic of low spin configuration of Co^{3+} while paramagnetic transition can be seen at higher temperature due to spin state transition to intermediate spin (IS) or high spin (HS) state. The magnetic species population rather develops in a broad temperature range. Thus $LnCoO_3$ have their magnetic transitions happening in a broad temperature region. The range for $LaCoO_3$ is 50-150 K [12]. For $YCoO_3$, it is 450-600 K [12]. For $LaCoO_3$, exact spin state nature is still uncertain, transition to intermediate spin (IS) is favoured by electron structure Local Density Approximation calculation [13] while Hartree-Fock calculation as well as Generalised Gradient Approximation calculation (GGA+U) is supportive of LS-HS pair stabilization [14-15]. In comparison, the nature of spin state transition with temperature for $YCoO_3$ has been studied by using *ab-initio* density functional calculation with Local Spin Density Approximation (LSDA) and LSDA+U methods [16]. Another unavoidable magnetic feature that is seen is the presence of paramagnetic moment at low temperature which can be seen for the whole series. The anomaly has been ascribed to collective effect of Curie like term and Van Vleck paramagnetism originating from field induced admixture state coming mainly from surface

Co [12, 17]. The magnetic transitions for $LnCoO_3$ systems are always accompanied with large change in resistivity which has been termed as Insulator-Metal (I-M) transition. As for the trend it has been seen that the magnetic and I - M transitions shift to higher temperatures in a systematic fashion with decrease in Ln_{ionic} radius. The I - M transition for $LaCoO_3$ is at around 500 K and for $YCoO_3$ it is at around 750 K [12]. $YCoO_3$ has nonmagnetic (spin S = 0) insulator type nature in the low temperature range and semiconductor type nature in the high temperature range (600-1000 K) with an electronic transition of Co^{3+} ion from low-spin state to high-spin state. The transition is registered by activation energy peak E_A which shifts its position according to the size of the Ln^{3+} considered. One more important feature of $LaCoO_3$ is presence of ferromagnetism in both nano and bulk phase powder and single crystals [17-18]. The bulk phase ferromagnetism has been assigned to the surface contribution while that of nanoscale $LaCoO_3$ is said to be originating from the reduction of Jahn-Teller distortion value [17-18]. Further people have tried to dope the Ln ion and see its effect on magnetism, band diagram, conductivity etc., $La_{0.5}Sr_{0.5}CoO_3$ being a well-known example of that [19].

4.2

Scope of present investigation:

Perovskite oxides have a tendency to release oxygen and thereby create oxygen deficiency. These deficiencies have very interesting impact on the crystal structure as well as band structure and thus often seen to be altering properties of the respective compound. Thus the defects or vacancies are sometimes very much on the wish list of the experimentalist. The deficiency gets created in different mechanisms *e.g.* during synthesis, during modification after synthesis. High temperature sintering during synthesis or heating in low partial pressure of oxygen are potential techniques of creating oxygen deficiency. Partial pressure of oxygen can be lowered via treatment of sample in inert or reducing atmosphere or in high vacuum condition. $YCoO_3$ as mentioned has unique fingerprint magnetic and electrical transition as

mentioned above. Present aim of our study is to create some oxygen deficiency in the compound and study what all effects it can have.

4.3

Experimental Section:

4.3.1 Chemicals:

Yttrium oxide (Y_2O_3) was purchased from Sigma Aldrich chemicals. Chromium nitrate hexahydrate [$Co(NO_3)_2$. $6H_2O$] and Citric acid ($C_6H_8O_7$) was purchased from SDFCL. All the reagents were AR grade. Yttrium oxide like other rare earth oxides had to be preheated at 900°C in air for 12 hours in order to remove the CO and moisture adsorbed at the compound surface. The deionized water with resistivity in the range of MΩ obtained from Millipore ultrapure water purification system.

4.3.2 Synthesis:

In 50 mL of deionized water, 0.8648 gm (3.829 mmol) of Y_2O_3 was added and was dissolved via drop wise addition of conc. HNO_3 into the solution. Under constant stirring 2.2291 gm (7.659 mmol) of $Co(NO_3)_2.6H_2O$ was added into the solution followed by addition of 2.2074 gm (11.489 mmol) of Citric Acid. Thus the citric acid concentration was exactly the double of total cation concentration. The whole solution was kept exposed to air under continuous stirring at 98°C such that solvent water evaporates slowly as well as the citrate complex gel precursor gets formed. This resultant gel precursor was then heated and dried for 12 hrs at 200°C. The product obtained was heated at 920°C at a rate of 5°C /min in oxygen flow for 5 hours in order to drive off the amorphous carbon in the form of CO_2. For magnetic and electrical measurement purpose, the product obtained so far was sintered at the same temperature for 10 hrs.

4.3.3 Characterization:

The products were characterized by X-ray diffraction technique using Bruker Discover D8 advance diffractometer and PANalytical Empyrean single wavelength ($K_{\alpha 1}$) diffractometer at room temperature and ambient atmosphere. Field-emission scanning electron microscope (FESEM) images and energy-dispersive analysis of X-rays (EDAX) were obtained by use of FEI (Nova-Nano SEM-600 Netherlands) instrument. Magnetic measurements were performed using vibrating sample magnetometer SQUID by Quantum design. High temperature FC and ZFW was measured in presence of external DC field of 5 kOe from 300 K to 1000 K. Low temperature FC and ZFC measurements were carried out in presence of following external dc fields: 10 Oe, 100 Oe, 1000 Oe, 5000 Oe from 2 K to 300 K. M vs H measurements were carried out at different temperatures in between the range of 2 K to 300 K. DC resistivity measurements were carried out in the temperature range of 10 K to 330 K in electrometer equipped with PPMS using two probe method.

4.4
Results and discussion:

4.4.1 Synthesis:

$YCoO_3$ can be prepared both in solid state [12] and sol-gel route [20]. The reported solid state route results in formation of Y_2O_3 impurity along with $YCoO_3$ while sol-gel route results in pure phase product at certain calcination temperature (optimum temperature) [20]. Calcination below the optimum temperature yields Y_2O_3 as impurity phase while calcination at above optimum temperature

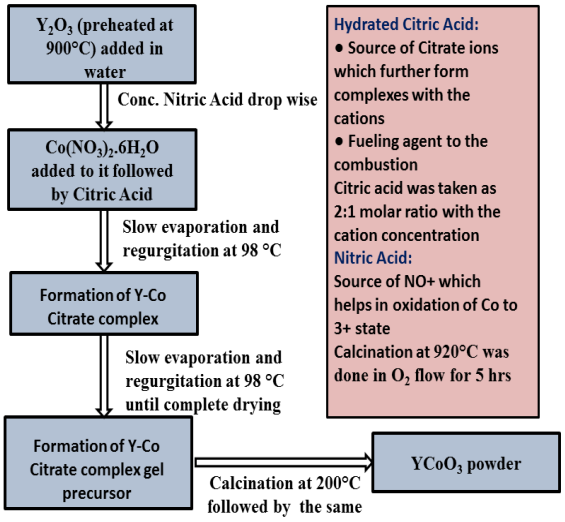

Figure 4.2.: Outline of $YCoO_3$ synthesis

results in formation of Co_3O_4 as the impurity phase. Thus calcination was carried out at 920°C and the product so obtained was considered for further studies. The Y_2O_3 was dissolved in water with addition of nitric acid drop wise which hydrolysed the oxide into Y^{3+} and NO_3^-. Citric acid was used as complexing agent as well as fuel. It has flash point at around 200°C. Figure 4.2. shows

4.4.2 Crystal Structure:

At room temperature and ambient atmosphere, compound was found to be crystallizing in distorted perovskite in orthorhombic symmetry with space group *Pbnm* {c.f. figure 4.3. (b)} Rietveld refinement plot along with the structure has been shown in figure 4.3. (a). The Structure comprises of CoO_6^{3-} octahedra not in regular fashion but distorted.

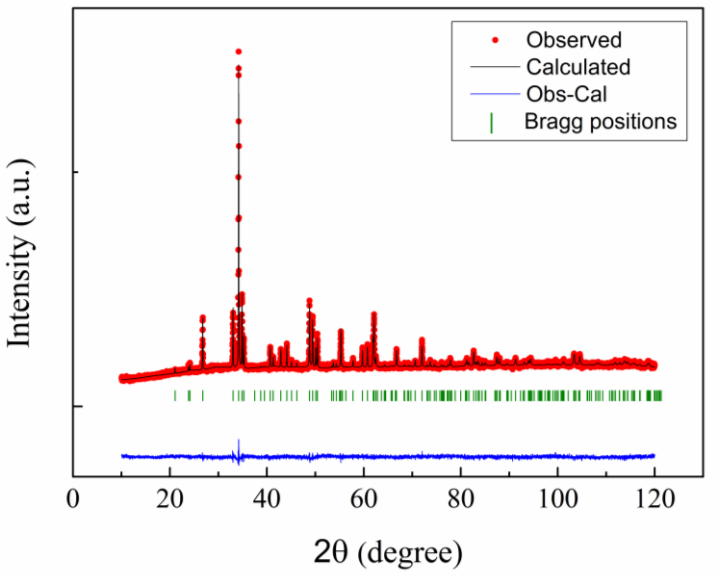

Figure 4.3. (a) Reitveld refinement plot of $YCoO_3$

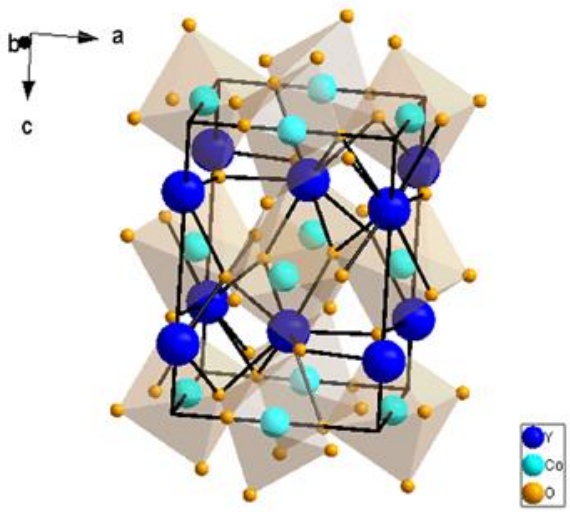

Figure 4.3. (b) Structure of $YCoO_3$ showing orthorhombic arrangement along with tilted Co-O octahedra.

Table 4.1.

Parameters	**A**	**b**	**c**	**c/√2**	**α**	**β**	**γ**
Magnitude	5.1388(1)	5.4205(7)	7.3668(3)	5.2091(3)	90.00	90.00	90.00

Thus, it can be seen that **b** > **c**/√**2** > **a**, which tells that the structure is of O-type where buckling of octahedral affects orthorhombic distortion [12]. The grain size of the non-sintered sample was calculated using Scherrer formula [21]. The peaks of 112 (most intense), 220 (second) and 111 (fifth) were selected. Results have been shown in table 4.2. The calculated grain size was found to be in the order of 150 nm.

Table 4.2.

Miller Indices	**112**	**220**	**111**
2θ (°)	34.187	48.8	26.772
Widths	0.08959	0.08984	0.09951
Sizes (nm)	161.91	154.32	143.28

The Scherrer formula does not hold good for compounds with grain size greater than 0.1 μm. Thus the above calculations were considered suspicious and the validity was checked by comparison with FESEM micrographs.

4.4.3 Morphology:

Figure 4.4. [(a) & (b)] show FESEM images of the non-sintered and sintered compound respectively. Irregular shaped particle of the size in μm range were observed. Average grain size was found to be around 0.5 μm for non-sintered sample while for sintered grain size almost doubled to an average value of around 1 μm. Thus the increment in size with sintering is clearly visible. This is because sintering brings particles closer to each other which leads to the increase in the extent of thermal diffusion. Thus more agglomeration occurs. Moreover the grain size values infer that the calculation of grain size with the help of

Scherrer formula will not be applicable for this as synthesized compound as the grain size is much higher than the upper limit of accuracy (0.1-0.2 μm).

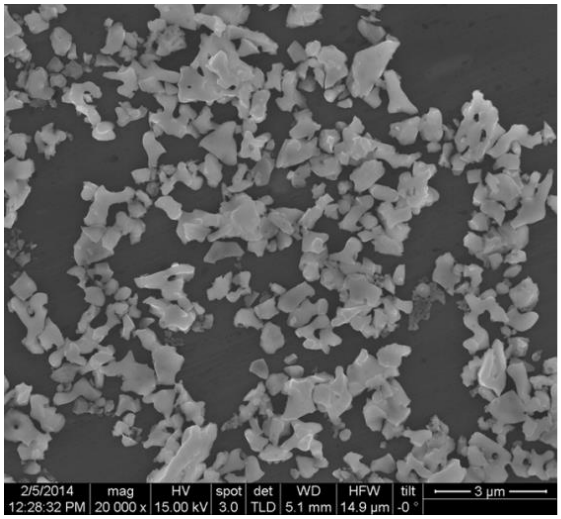

Figure 4.4. (a) SEM image of non-sintered $YCoO_3$ powder

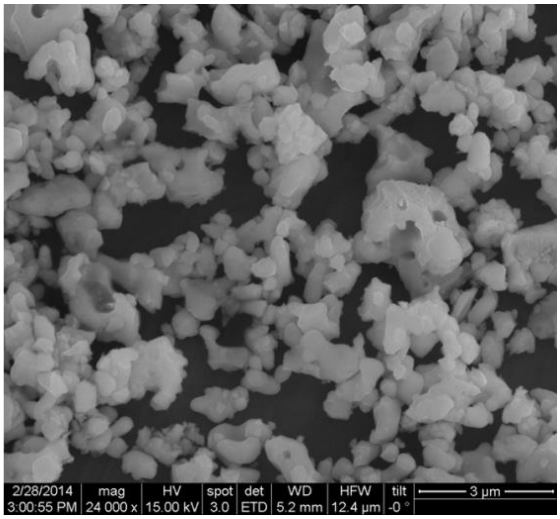

Figure 4.4. (b) SEM image of sintered $YCoO_3$ powder.

4.4.4 Magnetic Properties:

FC and ZFC measurements in presence of 1000 Oe external magnetic field in the temperature range of 2-300 K reveals that intrinsically diamagnetic $YCoO_3$ has considerable paramagnetic components and Curie like term associated with it {c.f. figure 4.5. (a)}. This has been ascribed to the effect of surface Co components forming field induced admixture states along with contribution of defect moments [12]. Temperature dependent diamagnetic component coming from core level elctronic contribution is also present. The M vs H measurement at 2 K with oscillating field of 50 kOe amplitude reveals presence of

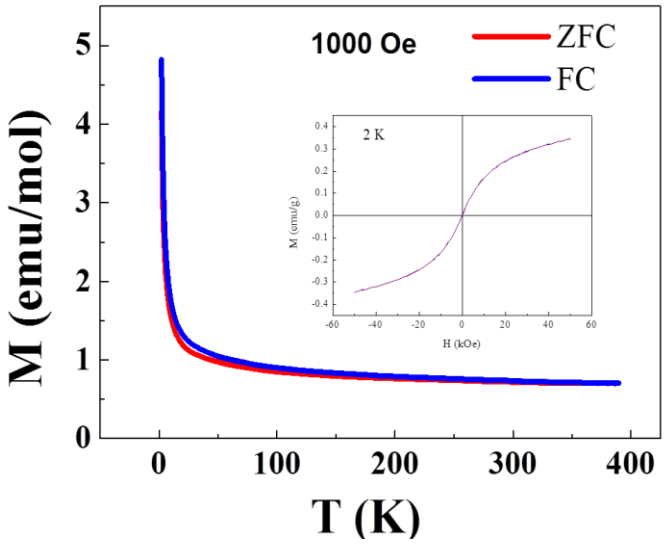

Figure 4.5. (a) FC & ZFC curves of powder $YCoO_3$ (1 kOe). (Inset) M vs H at 2 K

ferromagnetism of very dilute nature. Reason behind this is unknown. Chances of oxygen deficiency being present which might result into generation of ferromagnetic polarization can not be ignored. Presence of ferromagnetic impurity might also be a possible origin but XRD looked completely clean though.

As compared to the FC & ZFC data of sintered compound {c.f. figure 4.5. (b)}, reduction of moment value is seen along with an anomaly at 58 K. The anomaly corresponds to crystallization of oxygen and associated transition between paramagnetic to antiferromagnetic phase. Oxygen is paramagnetic in nature above 44 K and below this, antiferromagnetic ordering happens. Again O_2 freezes at 54 K. Often this freezing and ordering happen concurrently. This can be avoided by thorough purging at 320 K as well as by avoiding porous mounting materials. Porous compounds also tend to show this kind of behaviour due to adsorbed oxygen in the pores.

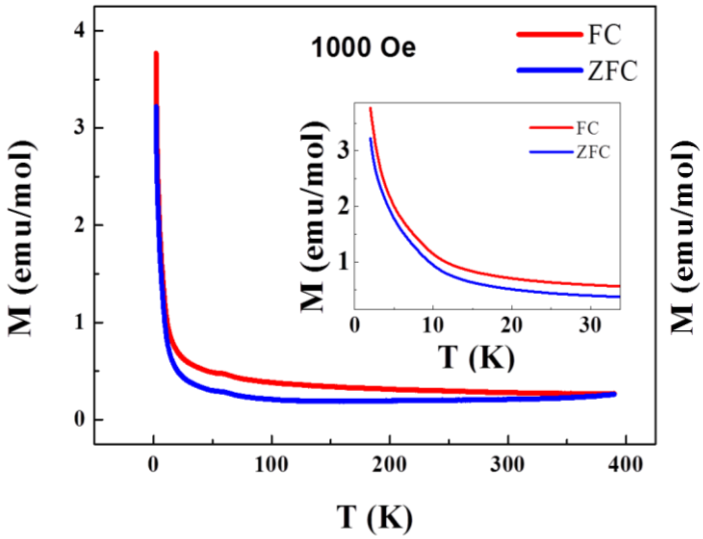

Figure 4.5. (b) FC & ZFC curves of sintered $YCoO_3$ (1000Oe). Inset zoomed view in the range of 2-30K.

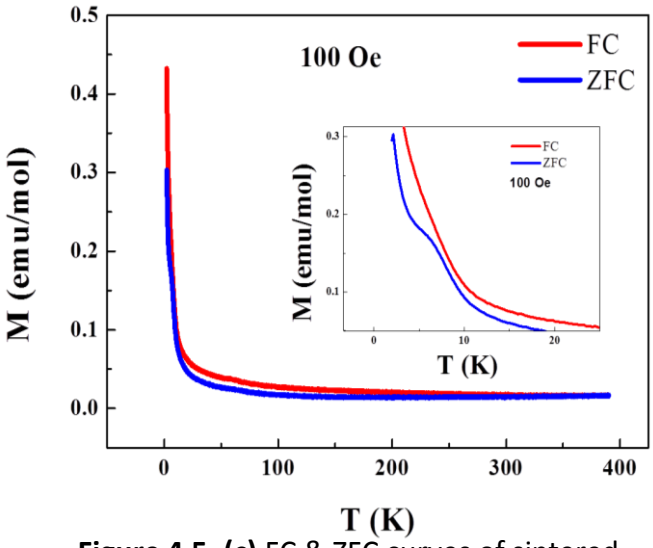

Figure 4.5. (c) FC & ZFC curves of sintered $YCoO_3$ (100Oe). Inset zoomed view in the range of 2-30 K.

Comparative study of the two plots {c.f. fig. 4.5. (b) and (c)} infers that at around 7 K one cusp like anomaly originates which is much more prominent at low external field and shifts to lower temperature on reduction of external field. At high field this anomaly completely vanishes as seen at 1000 Oe. The inconsistency of the cusp with respect to temperature tells

that the anomaly is not due to any characteristic temperature of any compound like T_C or T_N. Although there is no significant divergence between FC and ZFC, complete convergence was not seen either. The cusp thus may be due to formation of any glassy state. More studies on ac susceptibility, aging effect or memory effect is required to come into further conclusion. The M vs H measurements {c.f. fig. 4.5. (d), (e), (f) and (g)} have revealed presence of ferromagnetism in the compound although of very weak nature. None of the curves is seen to be getting saturated. The reason behind this is presence of paramagnetic moment along with ferromagnetic moment. Absence of any transition or anomaly which can account for the cusp {c.f. figure 4.5. (c)} strengthens possibility of presence of glassy state. The curves at 100 K and 300 K are very much representative of the presence of ferromagnetism in the compound. At low temperatures the moment is much more which gets reduced for measurement at high temperature. Compound shows higher value of coercivity at 100 K than at 300 K, remanent magnetization does not change although.

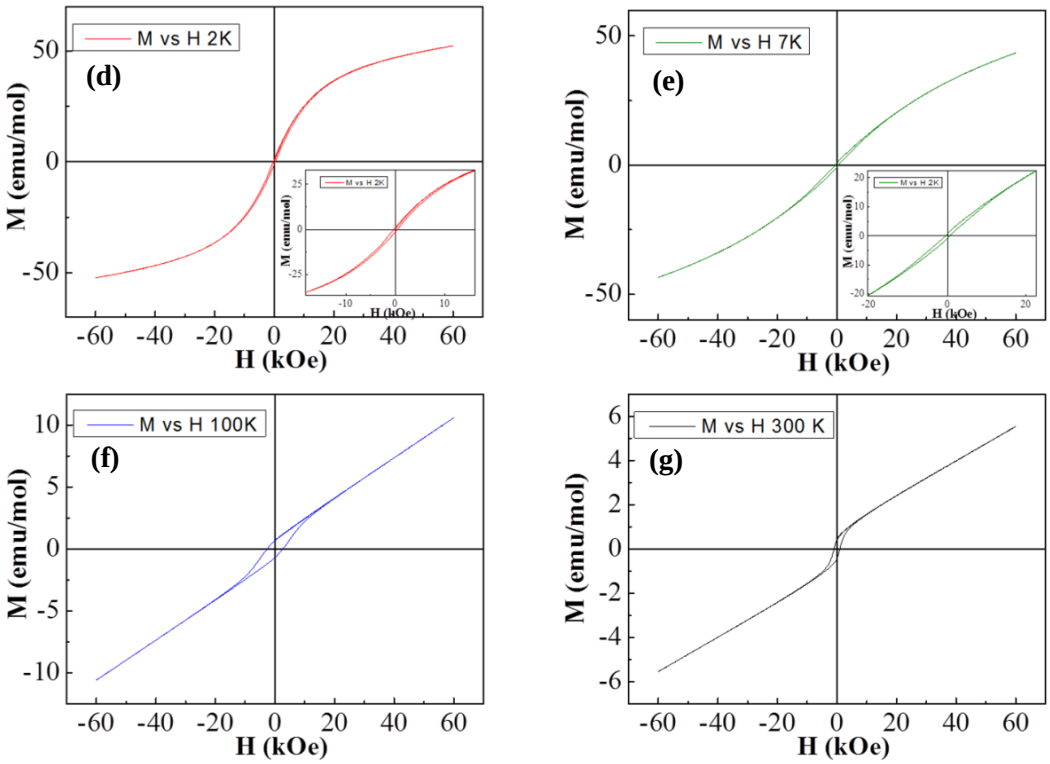

Figure 4.5. (d,e,f,g) M vs H curves of stoichiometric $YCoO_3$ measured (only at low temperature) at 2 K, 7 K, 100 K and 300 K. Inset panels show zoomed view of the loop.

The most prominent and interesting feature that was observed was during measurement of the sintered sample in high vacuum condition in the temperature range of 300-1000 K. In this temperature range, zero field warming (ZFW) and field cooled cooling (FCC) at 5000 Oe were carried out which produced unique and discreet behaviour. The increase in moment followed a certain path during ZFW {red curve fig 4.5. (h)} but during FCC {blue curve fig 4.5. (h)} it did not decrease following the same. The same measurement was repeated on the same pellet (i.e. the pellet on which the first ZFW followed by FCC were carried out) and it was seen to be following the FCC path with almost no significant difference between Field Warming (FW) and FCC {red & blue curve fig 4.5. (i)}.

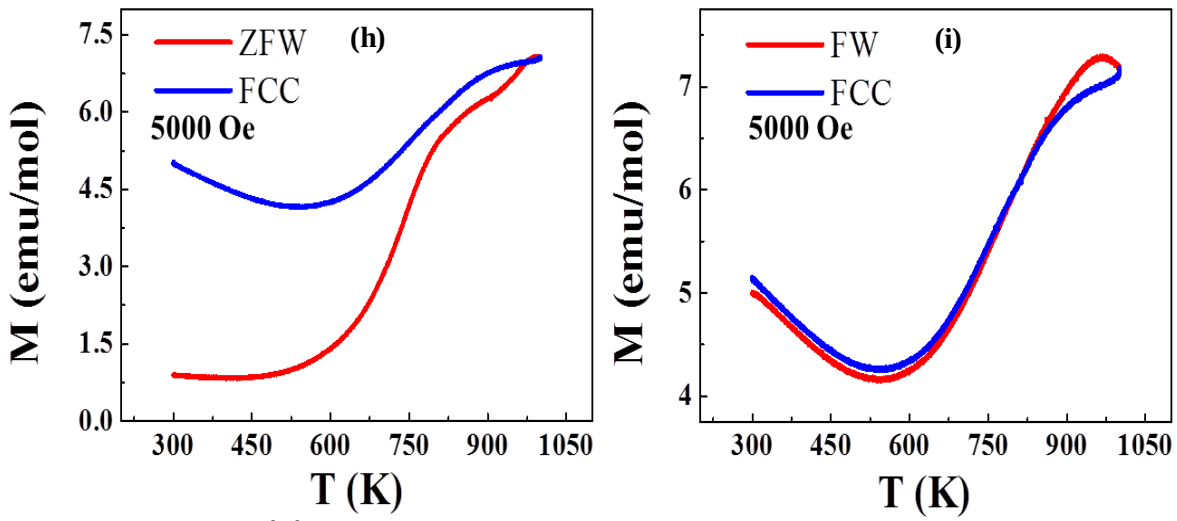

Figure 4.5. (h) First measurement data showing ZFW and FCC curves of sintered sample at 5000 Oe. **(i) Second measurement** data showing that the FCC path being followed, not the ZFW path.

Thus the following statement holds a strong ground: During ZFW certainly some change has occurred in the material on study which caused the observable change in moment and this change is an irreversible process as can be seen from the aspect of repeat measurement data. Perovskite oxides have a tendency to release some amount of oxygen thereby creating oxygen deficiency. The release of oxygen can be more probable if one reduces the external partial oxygen pressure by creating an inert/reducing atmosphere or by creating high vacuum. In present study, the change during high temperature can then be

strongly ascribed to oxygen release from the sample thereby creating lattice defects in it. This stoichiometry change results in increasing moment value.

The low temperature magnetic measurement of this nonstoichiometric sample did show peak like nature at 300 K which does not get suppressed at higher field {c.f. figure 4.5. (j, k)}. Absence of any secondary phase in the x-ray data of the same nonstoichiometric sample prompts us to consider this anomaly as inherent of the compound only but not contribution of any secondary phase.

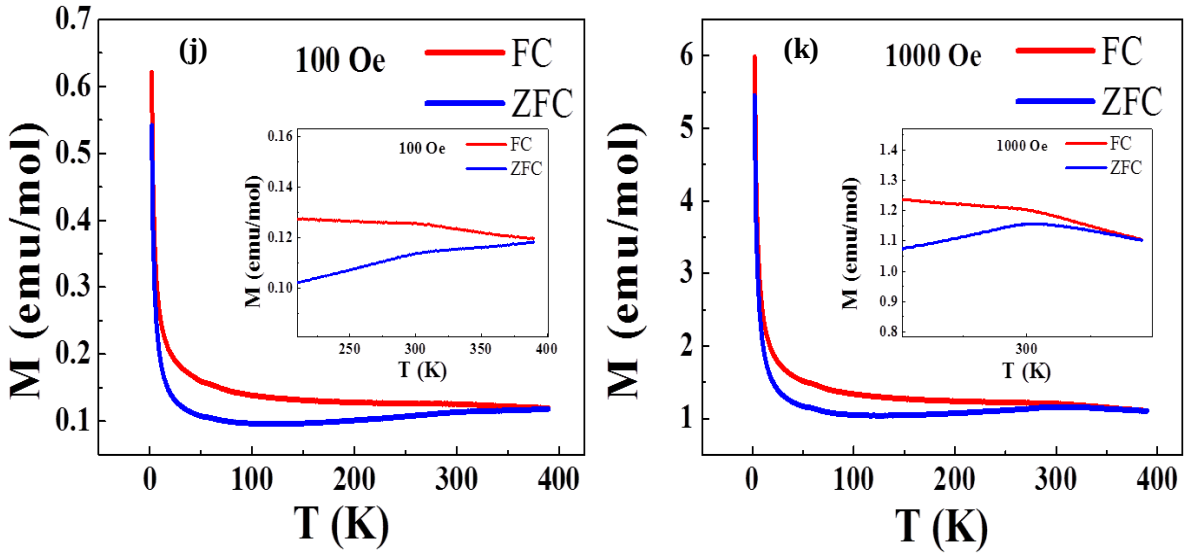

Figure 4.5. (j, k) FC & ZFC data (100 and 1000Oe) of the pellet measured at high temperature earlier. Insets show observed anomaly observed at 300 K.

The M vs H data {c.f. figure 4.5. (l, m, n, o) } for this nonstoichiometric sample has been shown below. Apart from the increase in overall moment and change in the, no distinguishable change was seen when compared with that of stoichiometric sample data {c.f. figure 4.5. (d, e, f, g) }. Paramagnetic contribution was seen along with weak ferromagnetism which prevented attainment of saturation.

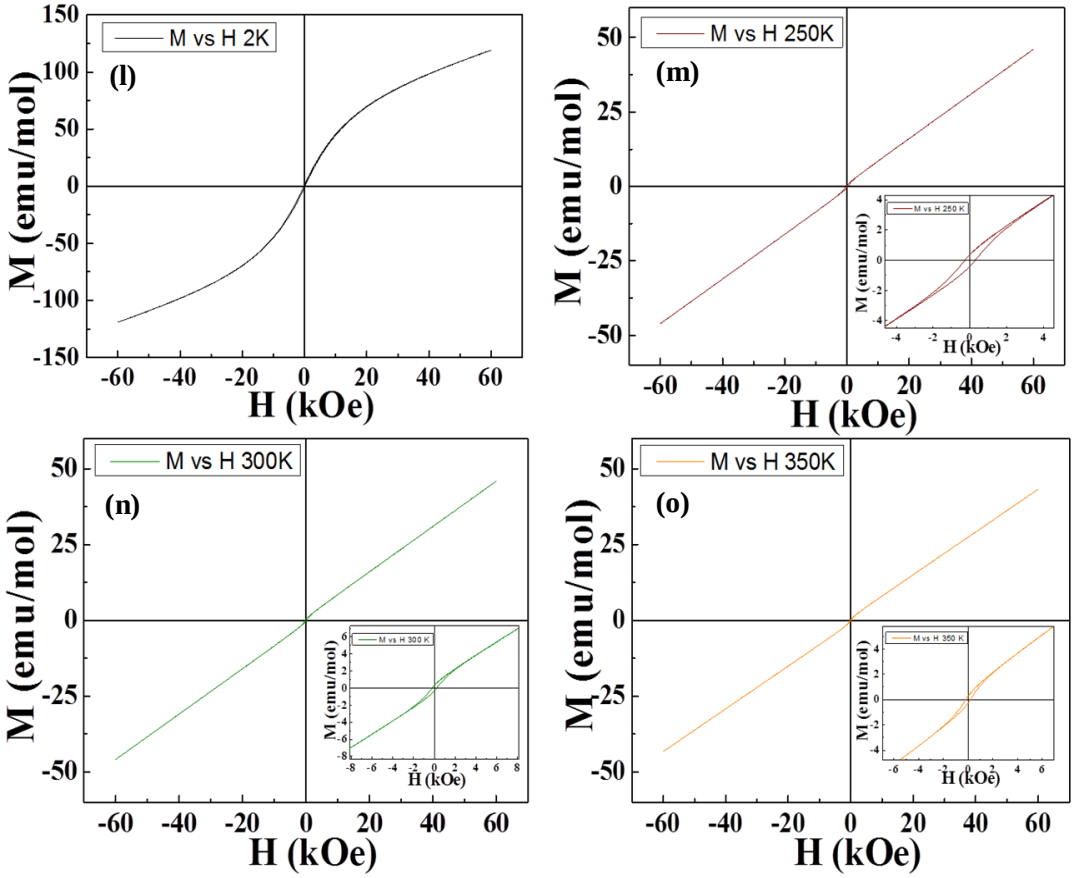

Figure 4.5. (l, m, n, o) M vs H curves of nonstoichiometric $YCoO_3$ measured (after high temperature measurement) at 2 K, 250 K, 300 K and 350 K. Inset panels show zoomed view of the loop.

4.4.5 Electrical Properties:

The resistivities of both stoichiometric and nonstoichiometric samples were measured from 10- 330 K at appropriate voltages. Looking at the nature of the curves and the respective values of resistivity it can be inferred that both the forms of the compound are semiconducting in nature.

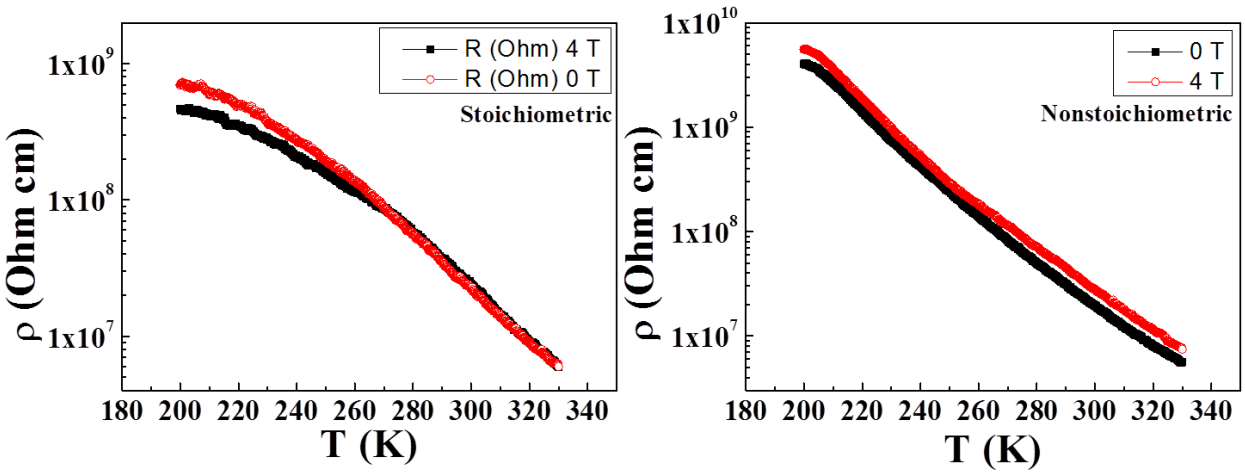

Figure 4.6. (a, b) ρ vs T (K) plots of nonstoichiometric $YCoO_3$ measured (after high temperature measurement) at external magnetic field of 0 T and 4 T.

4.5

Conclusion:

Thus in conclusion we have synthesized $YCoO_3$ via sol-gel method and characterized different properties. We have found few additional magnetic features compared to the stoichiometric compound [12] both at high and low temperature. The high T features evolved when compound was heated at high vacuum with concurrent magnetic data recording which prompts us to tell that the features are most probably due to change in stoichiometry (most probably release of oxygen) although myriad of experiments are to be done in order to ascertain that. The increase in moment of the sample after high vacuum heating as compared to non-heated sample supports the stoichiometry change only. In coming days we aim to carry out confirmative study like ac susceptibility, aging effect, or iodometric titration in order to know the exact reason behind this.

4.6

Bibliography:

1. Raveau, Bernard; Seikh, Md. Motin; Cobalt Oxides: From Crystal Chemistry to Physics, First Edition. Wiley-VCH Verlag GmbH & Co. KGaA, 2012.
2. Demazeau G. *et al.* (1974) J. Solid State Chem. **1974**, 9, 202.
3. Seikh, M. M.; Raveau, B.; Giant Magnetoresistance: New Research (eds Adrian D. Torres and Daniel A. Perez), NOVA Publishers, pp. 107, 2009.
4. Rao C. N. R. *et al.*, Top. Curr. Chem. **2004**, 234(II), 1.
5. Ivanova, B. N. *et al.*, Physics-Uspekhi **2009**, 52, 789.
6. Thornton, G. *et al.*, J. Solid State Chem. **1986**, 61, 301.
7. Raccah, P. M.; Goodenough, J. B.; Phys. Rev. **1967**, 155, 932.
8. Kappatsch, A. *et al.*, J. Phys. France **1970**, 31, 369.
9. Yakel, H. L.; Acta Crystallogr. **1955**, 8, 394.
10. Wold, A.; Ward, R.; J. Amer. Chem. Soc. **1954**, 76, 1029.
11. Zhou, J. -S. *et al.*, Phys. Rev. Lett. **2005**, 94, 06550.
12. Fjellvag, H. *et al*., Phys. Rev. B **2006**, 73, 214443.
13. Korotin, M. A.; Ezhov, S. Y.; Solovyev, I. V.; Anisimov, V. I.; Khomskii, D. I.; Sawatzky, G. A.; Phys. Rev. B **1996**, 54, 5309.
14. Zhuang, M.; Zhang, W.; Ming, N.; Phys. Rev. B **1998**, 57, 10705.
15. Knížek, K.; Jirák, Z.; Hejtmánek, J.; Novák, P.; J. Phys. Con. Matter **2006**, 18, 3285.
16. Zhu., Zhili; Guo., Juan; Jia, Yu; Xing, Hu; Physica B **2010**, 405, 359.
17. Goodenough, J. B. *et al*, Phys. Rev. B **2004,** 70, 014402.
18. Zhang *et al.*, Phys. Rev. B **2007**, 76, 172407.
19. Roy, B.; Das, S.; Journal of Alloys and Compounds **2011**, 509; 5537.

20. Xu, Dapeng *et al.* Phys. Status Solidi A **2012**, 209, No. 7, 1219.

21. Li, J. F.; Liao, H.; Wang, X. Y.; Coddet C.; Chen, H.; Ding, C. X.; Thin Solid Films **2004**, 460, 101.